Electronic Supplementary Material (ESI) for Nanoscale.

Electronic Supporting Information (ESI)

Fist-principles Structure Prediction of Two-dimensional HCN Polymorphs obtained via Formal Molecular Polymerization

Heng Zhang,[a,b] Junjie Wang,*[a] Frédéric Guégan,[b] Gilles Frapper*[b]

[a]State Key Laboratory of Solidification Processing, School of Materials Science and Engineering, Northwestern Polytechnical University, Xi'an, Shaanxi 710072, People's Republic of China. E-mail: wang.junjie@nwpu.edu.cn; heng.zhang@univ-poitiers.fr
[b]Applied Quantum Chemistry group, E4, IC2MP, UMR 7285 Poitiers University-CNRS, 4 rue Michel Brunet TSA 51106 - 86073 Poitiers Cedex 9, France. E-mail: gilles.frapper@univ-poitiers.fr;frederic.guegan@univ-poitiers.fr

Correspondence and requests for materials should be addressed to Junjie Wang (wang.junjie@nwpu.edu.cn), and Gilles Frapper (gilles.frapper@univ-poitiers.fr).

CONSTENT

S1 Methodology

S1.1 Evolutionary algorithm (USPEX)

USPEX (Universal Structure Predictor: Evolutionary Xtallography, version 10.3 and 9.4.4) is a global evolutionary search algorithm for crystal structure prediction developed by the A. R. Oganov laboratory since 2004 (see http://uspex-team.org/en/uspex/overview).[1, 2, 3, 4, 5] In this work, this evolutionary algorithm (EA) code is interfaced with VASP (Vienna Ab initio Simulation Package, version 5.4.4) for DFT structure relaxation (shape, volume, atomic positions are optimized by VASP). [6, 7] First, 2D fixed-composition EA search in USPEX was employed to predict the 2D HCN structures. In 2D fixed-composition EA searches, the thickness of 2D HCN structures is constrained up to 5 Å and the total number of atoms in the 2D unit cell is up to 24. The vacuum size is set to 20 Å. Besides, the seeds technique was used for 2D fixed-composition EA search. 2D HCN structures were obtained by the substitution of CH units of 2D graphane[8, 9] by N atoms. Second, we carried out molecular crystal EA searches at 0 GPa implemented in USPEX code to locate the most stable *van der Waals* HCN phase. The hydrogen cyanide molecule *HCN* and its isomer *HNC* were specified as the input of molecular crystal EA searches for 2D HCN- and HNC- based 2D nets. Up to 36 atoms were allowed in the primitive cell. Each USPEX job is run at least twice to ensure the convergence to a stable structure. Finally, 37 2D HCN crystals were obtained by 2D fixed-composition EA search and from 2D-lamellar structures obtained in bulk-EA searches. Our crystal searches reproduced the 2D HCN structures, i.e., *Pm*-I, *Pg*-I and *P*3*m*1 HCN[10].

A large number (120) of randomly created structures is chosen in the first generation of the EA. In the next generations, 100 structures are generated. The fitness is computed as the enthalpy (at T = 0K, G = H) derived from an *ab initio* total energy calculation (here DFT GGA PBE as implemented in VASP). All structures are then tested against three constraints: interatomic distances, cell angles and cell lengths. 80% of the best (i.e., lowest enthalpy) optimized structures are selected to participate in producing the next generation. New candidate structure is produced from parent structures using one of four operators defined in Refs 1-5: (i) heredity, (ii) lattice mutations, and (iii) atomic mutation, which account for 50, 10, and 20% of the structures in the new generation. The remaining 20% are randomly generated (similarly to those of the first generation). A fixed-composition EA search is considered achieved when the same global structure minimum is found during 10 consecutive generations. Typically, such search requires between 10 and 20 generations.

S1.2 DFT calculations (VASP)

Structural optimization. First-principles calculations are performed using the projected-augmented-wave (PAW) method as implemented in VASP (version 5.4.4).[6, 7] Exchange-correlation energy is treated using Perdew-Burke-Ernzerhof (PBE) within the generalized gradient approximation (GGA).[11, 12] In USPEX calculation, 5 successive steps of increasing convergence accuracy are usually required (i.e., 5 INCAR files). The parameters and criterion associated with VASP calculations then correspond to the last (5th) step of the highest accuracy (given thereafter). A kinetic cutoff energy of 600 eV is used for the wavefunction expansion with a Monkhorst-Pack k mesh grid with a spacing of $2\pi\times0.04$ Å^{-1}. This ensure that enthalpy converges to a criterion lower than 1×10^{-5} eV per cell, and forces to 0.01 eV/Å. The valence electron configurations considered in the calculation are H($1s^1$), C($2s^22p^2$), N($2s^22p^3$), Si($3s^23p^2$), Ge($4s^24p^2$), F($2s^22p^5$), Cl($3s^22p^5$), S($3s^22p^4$), P($3s^23p^5$), and Mo($4p^65s^14d^5$). As one would expect with these elements and compositions, no magnetism is observed in all 2D-HCN, HNC and related isovalent phases (all ground states are non-magnetic, as shown by spin-polarized calculations). Therefore, hereafter all calculations are non-spin-polarized.

Energy band gap. PBE functional has proven to be accurate for the description of structural properties of materials.[13] In contrast, it may underestimate the value of the band gaps. Therefore, we calculated the band gap at the Heyd-Scuseria-Ernzerhof (HSE06)[14] hybrid functional level of theory, using the optimized PBE structure (single-point energy calculation). This level of theory is noted thereafter as HSE06//PBE. During the band gap calculation, twenty k-points were used between two high-symmetric K-points in the reciprocal space (Γ-Y-S-X-Γ), i.e., Γ(0 0 0), Y(0.5 0 0), S(0.5 0.5 0), and X(0 0.5 0).

Chemical bonding analysis. To study the chemical bonding, density of states (DOS), and Manz bond order (Chargemol program)[15] from the optimized geometries were also analyzed.

Structural parameters analysis and images. Finally, images of the crystalline structures were produced using VESTA software.[16]

S1.3 Phonon dispersion calculations

In this work, first principles phonon calculations with density functional perturbation theory (DFPT) at a quasi-harmonic level were done using the open-source package PHONOPY (https://phonopy.github.io/phonopy/)[17] Supercells of 2D structures with displacements were created from a unit cell considering all possible crystal symmetry operations. In general, a 3×3 supercell is sufficient, but larger ones can be required to avoid unphysical imaginary frequencies needed.

The zero-point energy (ZPE) factor was calculated from the computed phonon frequencies ω_i under the quasi-harmonic approximation. ZPE is proportional to the sum over all phonon modes ω_i. The detailed theoretical methodology implemented in PHONOPY code is given in reference 17. The calculated ZPEs are listed in Tables S2, and S7-9.

S1.4 Mechanical properties

A necessary condition for the thermodynamic stability of a crystal lattice is that the crystal should be mechanically stable with respect to arbitrary (small) homogeneous deformations. Elastic stability criteria for bulk cubic crystals and more different crystal classes was well understood in the work of Born and co-authors.[18, 19, 20] The elastic tensor is determined by performing six finite distortions of the lattice and deriving the elastic constants from the strain-stress relationship.[21]

The elastic matrix of 2D materials was decreased into 3×3 and six elastic constants are C_{11}, C_{12}, C_{22}, C_{16}, C_{26} and C_{66} using the standard Voigt notation:*1*-xx, *2*-yy, *6*-xy. In 2D rectangular unit-cells, C_{16} and C_{26} are zero. The calculated elastic constants C_{11}, C_{12}, C_{22} and C_{66} in 2D materials should satisfy necessary mechanical equilibrium conditions for mechanical stability: $C_{11}C_{22}-C_{12}C_{21}>0$ and C_{11}, C_{22}, $C_{66}>0$.[22, 23]

In terms of these elastic constants, the 2D Young's moduli (in-plane stiffness) for the stain in the [10] and [01] direction are,[24, 25]

$Y_{21} = (C_{11}C_{22}-C_{12}C_{12})/C_{22}$, (eq.1)

$Y_{12} = (C_{11}C_{22}-C_{12}C_{12})/C_{11}$. (eq.2)

The corresponding Poisson's ratio are,[25]

$v_{12}=C_{12}/C_{22}$, (eq.3)

$v_{21}=C_{12}/C_{11}$. (eq.4)

In a 2D rectangular lattice (x, y), the in-plane Poisson's ratio $v(\theta)$ and Young's modulus $Y(\theta)$ along the in-plane θ can be expressed as follows,[24, 25]

$$\nu(\theta)=\frac{C_{12}\sin^4\theta-B\sin^2\theta\cos^2\theta+C_{12}\cos^4\theta}{C_{11}\sin^4\theta+A\sin^2\theta\cos^2\theta+C_{22}\cos^4\theta}, \qquad \text{(eq.5)}$$

$$Y(\theta)=\frac{C_{11}C_{22}-C_{12}C_{21}}{C_{11}\sin^4\theta+A\sin^2\theta\cos^2\theta+C_{22}\cos^4\theta}, \qquad \text{(eq.6)}$$

in which, $A=(C_{11}C_{22}-C_{12}C_{21})/C_{33}-2C_{12}$ and $B=C_{11}+C_{22}-(C_{11}C_{22}-C_{12}C_{21})/C_{33}$. The angle $\theta=0^{\circ}$ corresponds to [10] direction (x), and $\theta=90^{\circ}$ corresponds to [01] direction (y).

S1.5 *Ab initio* molecular dynamics simulations

Thermal stability. *Ab initio* molecular dynamics (AIMD) simulations based on DFT PBE calculations were carried out using VASP code to examine the thermal stabilities of 2D HCN and HNC structures. AIMD calculations with NVT ensemble and Andersen thermostat were performed at 400K and 800 K. The timestep was 1 *fs*, and the total simulation time was as long as 8 *ps*. In such AIMD simulations, 4×4 supercells of six proposed 2D HCN and HNC **1**-**6** phases were employed. The Brillouin zone integration was restricted to the Γ point of the supercell, due to a high calculation cost.

Pressure-induced *HCN* polymerization: en-route to 2D HCN nets. To explore the possible polymerization of *I*4*mm* hydrogen cyanide molecular crystal upon compression, AIMD simulations based on DFT PBE-D2[26] calculations at constant pressure-temperature conditions (NpT ensemble) were carried out using the Langevin thermostat.[27, 28] The precursor was first melted at specific temperatures (300, 350 and 400 K) at ambient pressure (P= 0 GPa), then the precursor was gradually compressed to 50 GPa (in 10 GPa-steps).[29, 30] At each pressure, NpT AIMD run for 4 ps with timestep of 1fs. The 3×3×3 (54 HCN units, 162 atoms per supercell) supercells of *I*4*mm* hydrogen cyanide phase were adopted to study the structural transformation, i.e., the polymerization process.

S2 Enthalpies and crystallographic parameters of 0D *HCN*-based molecules

Table S1 Calculated energies (eV/formula unit, f.u.) and crystallographic parameters (Å, °) of HCN hydrogen cyanide, HNC hydrogen isocyanide, $C_3H_3N_3$ 1,3,5-, 1,2,3- and 1,2,4-triazine molecules and their molecular crystals at ambient conditions at the PBE and PBE-D2 levels of theory

			PBE		PBE-D2	
		Space group	Energy (eV/f.u.)	Crystallographic parameters (Å, °)	Energy (eV/f.u.)	Crystallographic parameters (Å, °)
molecule	1,3,5-triazine		-20.624	C-N: 1.34 C-H: 1.09	-20.649	C-N: 1.34 C-H: 1.09
	1,2,4-triazine		-20.266	C-N: 1.33, 1.34 C-C: 1.40 C-H: 1.09	-20.292	C-N: 1.33, 1.34 C-C: 1.40 C-H: 1.09
	1,2,3-triazine		-20.057	C-N: 1.34 C-C: 1.39 N-N: 1.33 C-H: 1.09	-20.084	C-N: 1.35 C-C: 1.39 N-N: 1.33 C-H: 1.09
	HCN		-19.697	C-N: 1.16 C-H: 1.07 C-N: 1.158 C-H: 1.071[31]	-19.703	C-N: 1.16 C-H: 1.08
	HNC		-19.080	C-N: 1.18 N-H: 1.07 C-N: 1.18 N-H: 1.07[31]	-19.084	C-N: 1.18 N-H: 1.01
bulk	1,3,5-triazine	*R*-3*c* SG 167 Z=18	-20.687	a=b=9.884, c=7.902, α=β=90.0, γ=120.0	-20.865	a=b=9.467, c=7.036, α=β=90.0, γ=120.0 CCDC-1275718 a=b=9.647, c=7.281,

						α=β=90.0, γ=120.0[32]
	1,2,3-triazine	*P*-1 SG 2 Z=6	-20.172	a=5.836, b=7.467, c=5.791, α=107.4, β=112.5, γ=94.0	-20.359	a=5.679, b=6.549, c=5.580, α=110.7, β=114.4, γ=95.2 CCDC-1125638 a=5.769, b=6.873, c=5.672, α=110.1, β=113.9, γ=95.3[33]
	HCN	*I4mm* SG 107 Z=2	-20.014	a=b=4.850, c=4.264, α=β=γ=90.0,	-20.155	a=b=4.235, c=4.245, α=β=γ=90.0, a=b=4.63, c=4.34, α=β=γ=90.0[34]

S3 Enthalpies and crystallographic parameters of 2D HCN and HNC structures

Table S2 Calculated enthalpies (eV/f.u.), reaction energies and ZPEs of 2D HCN and HNC structures at the PBE level of theory (f.u., formula unit)

Family	Phase	Z	Space Group	Enthalpy (eV/f.u.)	ZPE (eV/f.u.)	Enthalpy (eV/f.u.)	Reference
				PBE		HSE06//PBE	
A	**1**	2	$Pmn2_1$ SG 31	-20.657	0.638	-24.649	Pm-I[10] PC7-2D[35]
	1b	4	$Pmc2_1$ SG 26	-20.593	0.633	-24.582	P2mg-I[10]
	1c	4	$Pca2_1$ SG 29	-20.506	0.636	-24.496	Pg-I[10]
	1d	1	$P3m1$ SG 156	-20.496	0.624	-24.480	P3m1[10] PC6-2D[35]
	1e	2	$Pmn2_1$ SG 31	-20.453	0.631	-24.441	Pm-II[10] PC4-2D[35]
	1f	12	$Pca2_1$ SG 29	-20.369	0.625	-23.780	
B	**2**	6	$Pma2$ SG 28	-20.358	0.633	-24.330	
	2b	6	$P2_1/m$ SG 11	-20.313	0.628	-24.283	
	2c	4	$Pmm2$ SG 25	-20.160	0.625	-24.110	
	2d	6	$P2_1/m$ SG 11	-20.139	0.627	-24.103	
C	**3**	4	$P2_12_12$ *SG 18*	-20.264	0.632	-24.231	
	3b	8	$P2/c$ SG 13	-20.247	0.631	-24.212	
	3c	2	$P2/m$ SG 10	-20.243	0.631	-24.202	
	3d	4	$P2_1/c$ SG 14	20.229	0.630	-24.193	
	3e	2	$P2/m$ SG 10	-20.175	0.633	-24.129	

	3f	2	$P\bar{1}$ SG 2	-20.034	0.603	-24.053	NPC7_2D[35]
	3g	4	$P2_1/c$ SG 14	20.017	0.627	-23.967	
	3h	4	$P2_1/c$ SG14	19.983	0.630	-23.931	
	3i	4	$Pmc2_1$ SG 26	19.970	0.631	-23.917	
	3j	4	$Pcc2$ SG 27	19.908	0.622	-23.859	
	3k	4	$P2/c$ SG 13	19.899	0.599	-23.733	
	3l	2	$Pmm2$ *SG 25*	19.830	0.615	-23.760	
	3m	4	$Pba2$ SG 32	19.742	0.613	-23.674	
D	**4**	6	Cm SG 8	20.124	0.627	-24.072	
	4b	6	$Pmn2_1$ SG 31	-20.113	0.628	-24.068	
	4c	6	$Pmc2_1$ SG 26	20.112	0.628	-24.066	
	4d	6	$Pmn2_1$_II SG 31	-19.910	0.626	-23.846	
E	**5**	4	$P222_1$ SG 17	-19.928	0.620	-23.822	
	5b	4	$P2/c$ SG 13	-19.911	0.624	-23.805	
	5c	2	$P2_1/m$ SG 11	-19.830	0.622	-23.734	
	5d	4	$P222_1$ SG 17	19.589	0.612	-23.454	
	5e	2	$Pma2$ SG 28	19.586	0.613	-23.503	
	5f	2	$P2_1/m$ SG 11	19.571	0.618	-23.457	
	5g	4	$P2_1/m$	19.558	0.619	-23.446	

			SG 11				
F	**6**	4	*Pbcm* SG 57	-20.655	0.641	-24.644	
	6b	4	$Pmc2_1$ SG 26	-20.637	0.639	-24.608	
	6c	2	*P*2/*m* SG 10	-20.633	0.639	-24.602	α-CNH[36]

Table S3 Crystallographic parameters of 2D HCN and HNC structures at the PBE level of theory

Family	Phase	Z	Space Group	Lattice parameters (Å,°)	Atomic coordinates (fractional)
A	**1**	2	$Pmn2_1$ SG 31	a=2.380, b=39.984, c=3.581, α=β=γ=90.0 a=2.355 c=3.514[10]	N 2a (0.500 0.014 0.868) C 2a (0.500 0.985 0.137) H 2a (0.500 0.961 0.987)
	1b	4	$Pmc2_1$ SG 26	a=2.381, b=22.708, c=7.227, α=β=γ=90.0 a=2.353 c=7.082[10]	H 2a (0.000 0.452 0.137) H 2b (0.500 0.408 0.872) C 2a (0.000 0.495 0.060) C 2b (0.500 0.452 0.802) N 2a (0.000 0.545 0.189) N 2b (0.500 0.499 0.943)
	1c	4	$Pca2_1$ SG 29	a=4.333, b=42.000, c=4.002 α=β=γ=90.0 a=4.259 c=3.945[10]	N 4a (0.599 0.012 0.852) C 4a (0.589 0.014 0.485) H 4a (0.996 0.962 0.412)
	1d	1	*P*3*m*1 SG 156	a=b=2.379, c=31.606 α=β=90.0, γ=120.0 a=b=2.381[10]	N 1a (0.667 0.333 0.735) C 1a (0.333 0.667 0.720) H 1a (0.333 0.667 0.684)
	1e	2	$Pmn2_1$	a=2.376,	H 2a (0.000 0.584 0.748)

			SG 31	b=17.562 c=4.018, α=β=γ=90.0 a=2.348, c=3.962[10]	C 2a (0.000 0.522 0.687) N 2a (0.000 0.515 0.319)
	1f	12	*Pca*2_1 SG 29	a=4.987, b=20.000, c=4.417, α=β=γ=90.0	C 4a (0.640 0.485 0.090) H 4a (0.690 0.432 0.120) N 4a (0.640 0.515 0.310)
B	**2**	6	*Pma*2 SG 28	a=7.169, b=3.614, c=19.416, α=β=γ=90.0	C 4d (0.913 0.118 0.468) H 4d (0.906 0.262 0.418) N 4a (0.917 0.383 0.526) C 2c (0.750 0.615 0.530) H 2c (0.750 0.757 0.581) N 2c (0.750 0.886 0.472)
	2b	6	$P2_1/m$ SG 11	a=4.130, b=7.168, c=16.995, α=β=γ=90.0	C 4f (0.588 0.416 0.515) H 4f (0.593 0.426 0.581) N 4f (0.920 0.415 0.483) C 2e (0.088 0.250 0.515) H 2e (0.072 0.250 0.581) N 2e (0.424 0.250 0.488)
	2c	4	*Pmm*2 SG 25	a=2.377, b=8.072, c=33.007 α=β=γ=90.0	N 2g (0.000 0.158 0.744) N 2h (0.500 0.408 0.730) C 2g (0.000 0.338 0.750) C 2h (0.500 0.097 0.723) H 2h (0.500 0.138 0.691) H 2g (0.000 0.362 0.783)
	2d	6	$P2_1/m$ SG 11	a= 17.487, b=7.158, c=4.020, α=β=γ=90.0	C 4f (0.477 0.917 0.430) N 4f (0.479 0.915 0.059) H 4f (0.417 0.929 0.505) C 2e (0.519 0.750 0.929) N 2e (0.513 0.750 0.561) H 2e (0.580 0.750 0.000)
C	**3**	4	$P2_12_12$ SG 18	a=4.782, b=3.620, c=19.375, α=β=γ=90.0	C 4c (0.866 0.119 0.532) H 4c (0.849 0.260 0.582) N 4c (0.122 0.614 0.473)

	3b	8	*P*2/*c* SG 13	a=4.780, b=22.364, c=7.312, α=β=γ=90.0	H 4g (0.129 0.451 0.124) H 4g (0.365 0.409 0.887) C 4g (0.124 0.545 0.195) C 4g (0.375 0.503 0.941) N 4g (0.130 0.496 0.060) N 4g (0.369 0.452 0.810)
	3c	2	*P*2/*m* SG 10	a=39.885, b=2.382, c=4.154 α=β=γ=90.0	N 2m (0.007 0.000 0.336) C 2n (0.006 0.500 0.825) H 2n (0.034 0.500 0.822)
	3d	4	$P2_1/c$ SG 14	a= 20.000, b=4.783, c=4.133, α=β=γ=90.0	N 4e (0.985 0.874 1.078) C 4e (0.987 0.129 0.590) H 4e (0.932 0.129 0.592)
	3e	2	*P*2/*m* SG 10	a=3.538, b=2.388, c=32.998 α=β=γ=90.0	N 2n (0.384 0.500 0.518) C 2m (0.857 0.000 0.482) H 2m (0.019 0.000 0.453)
	3f	2	$P\bar{1}$ SG 2	a=4.461, b=2.586, c=21.965, α=β=90.0, γ=105.7	H 2i (0.428 0.093 0.045) C 2i (0.072 0.282 0.005) N 2i (0.385 0.434 0.026)
	3g	4	$P2_1/c$ SG 14	a=22.708, b=4.020, c=4.777, α=β=γ=90.0	C 4e (0.484 0.930 0.871) N 4e (0.484 0.558 0.874) H 4e (0.437 0.010 0.873)
	3h	4	$P2_1/c$ SG 14	a=19.626, b=4.262, c=4.011, α=β=γ=90.0	C 4e (0.030 0.093 0.071) H 4e (0.077 0.513 0.485) N 4e (0.968 0.917 0.556)
	3i	4	$Pmc2_1$ SG 26	a=4.087, b=19.261, c=4.261, α=β=γ=90.0	C 4c (0.809 0.030 0.092) N 4c (0.315 0.970 0.912) H 4c (0.736 0.919 0.485)
	3j	4	*Pcc*2 SG 27	a=4.184, b=22.564, c=4.667, α=β=γ=90.0	C 4e (0.165 0.484 0.887) H 4e (0.128 0.436 0.939) N 4e (0.343 0.485 0.613)
	3k	4	*P*2/*c* SG 13	a=4.131, b=18.428, c=4.618,	C 4g (0.042 0.036 0.596) N 4g (0.599 0.949 0.381)

				α=β=γ=90.0	H 4g (0.887 0.920 0.953)
	3l	2	*Pmm*2 SG 25	a=2.371, b=4.104 c=17.232, α=β=γ=90.0	N 2g (0.000 0.683 0.517) C 2g (0.500 0.190 0.478) H 2g (0.500 0.742 0.414)
	3m	4	*Pba*2 SG 32	a=4.169 b=4.709, c=16.830, α=β=γ=90.0	C 4c (0.097 0.359 0.521) H 4c (0.127 0.307 0.586) N 4c (0.413 0.363 0.482)
D	**4**	6	*Cm* SG 8	a=4.133, b=7.192, c=16.930, α=β=γ=90.0	C 4b (0.337 0.171 0.515) H 4b (0.335 0.173 0.581) N 4b (0.172 0.335 0.484) C 2a (0.659 0.500 0.486) H 2a (0.655 0.500 0.421) N 2a (0.327 0.500 0.519)
	4b	6	*Pmn*2_1 SG 31	a=7.171, b=40.000, c=3.614 α=β=γ=90.0	N 4b (0.161 0.012 0.866) N 2a (0.000 0.011 0.635) C 4b (0.177 0.984 0.132) C 2a (0.000 0.982 0.372) H 2a (0.000 0.957 0.511) H 4b (0.196 0.959 0.989)
	4c	8	*Pmc*2_1 SG 26	a=7.181, b=16.777, c=7.299, α=β=γ=90.0	H 4c (0.826 0.378 0.883) H 4c (0.327 0.435 0.127) H 2a (0.000 0.617 0.101) H 2b (0.500 0.564 0.881) C 4c (0.828 0.436 0.808) C 4c (0.328 0.494 0.060) C 2a (0.000 0.562 0.185) C 2b (0.500 0.504 0.939) N 4c (0.835 0.503 0.942) N 4c (0.335 0.560 0.193) N 2a (0.000 0.492 0.061) N 2b (0.500 0.439 0.805)
	4d	6	*Pmn*2_1 SG 31	a=7.181, b=32.837, c=4.019 α=β=γ=90.0	N 4b (0.164 0.510 0.689) N 2a (0.000 0.487 0.804) C 2a (0.000 0.489 0.177) C 4b (0.171 0.511 0.317)

					H 4b (0.171 0.543 0.241) H 2a (0.000 0.458 0.268)
E	**5**	4	$P222_1$ SG 17	a=4.779, b=40.004, c=3.623 α=β=γ=90.0	N 4e (0.884 0.984 0.369) C 4e (0.368 0.985 0.367) H 4e (0.356 0.962 0.525)
	5b	4	$P2/c$ SG 13	a=32.698, b=4.795, c=4.160 α=β=γ=90.0	N 4g (0.509 0.879 0.587) C 4g (0.507 0.365 0.578) H 4g (0.541 0.357 0.574)
	5c	2	$P2_1/m$ SG 11	a=39.982, b=2.423, c=4.131 α=γ=β=90.0	N 2e (0.008 0.750 0.583) C 2e (0.007 0.250 0.087) H 2e (0.034 0.250 0.095)
	5d	4	$P222_1$ SG 17	a=22.315, b=4.649, c=4.246, α=γ=β=90.0	N 4e (0.519 0.132 0.591) C 4e (0.486 0.354 0.414) H 4e (0.438 0.288 0.392)
	5e	2	$Pma2$ SG 28	a=2.413, b=3.615, c=19.228, α=γ=β=90.0	N 2c (0.250 0.120 0.472) C 2c (0.750 0.622 0.532) H 2c (0.750 0.764 0.583)
	5f	2	$P2_1/m$ SG 11	a=17.264, b=2.416, c=4.021, α=γ=β=90.0	N 2e (0.523 0.750 0.557) C 2e (0.520 0.750 0.931) H 2e (0.580 0.750 0.012)
	5g	4	$P2_1/m$ SG 11	a=4.241, b=4.100, c=19.289, α=γ=β=90.0	N 4f (0.097 0.062 0.030) C 4f (0.576 0.438 0.967) H 4f (0.015 0.015 0.920)
F	**6**	4	$Pbcm$ SG 57	a=39.984, b=2.687, c=4.774 α=β=γ=90.0	N 4d (0.032 0.769 0.250) H 4d (0.046 0.444 0.250) C 4c (0.989 0.250 0.500)
	6b	4	$Pmc2_1$ SG 26	a=2.392, b=39.992, c=2.682, α=β=γ=90.0	N 2a (0.00 0.967 0.053) H 2a (0.000 0.046 0.880) C 2b (0.500 0.011 0.567)
	6c	2	$P2/m$ SG 10	a=2.681, b= 2.393, c=16.589, α=β=γ=90.0	H 2m (0.930 0.000 0.611) N 2m (0.730 0.000 0.421) C 2n (0.254 0.500 0.527)

				a=2.68, b=2.39[34]	

S4 Dynamical stabilities of 2D HCN and HNC structures

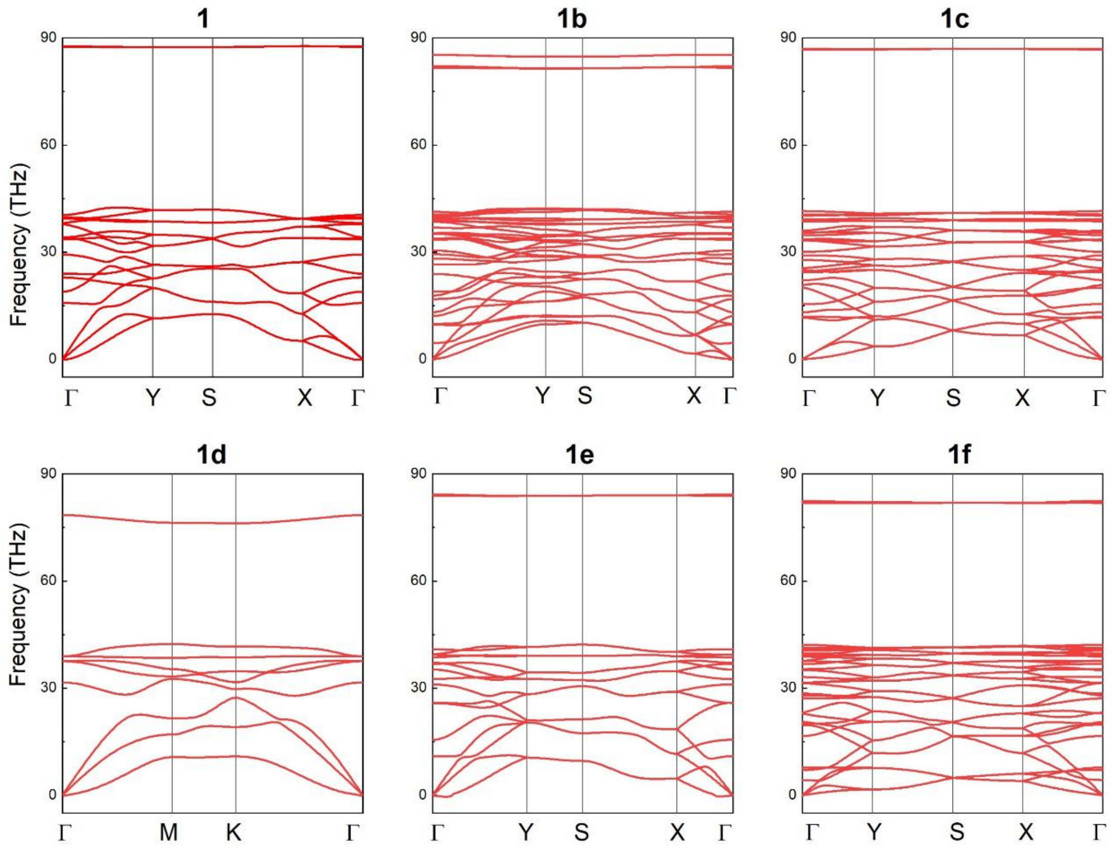

Figure S1 Phonon dispersion curves of 2D HCN structures of family **A**: **1** and **1b-f** phases

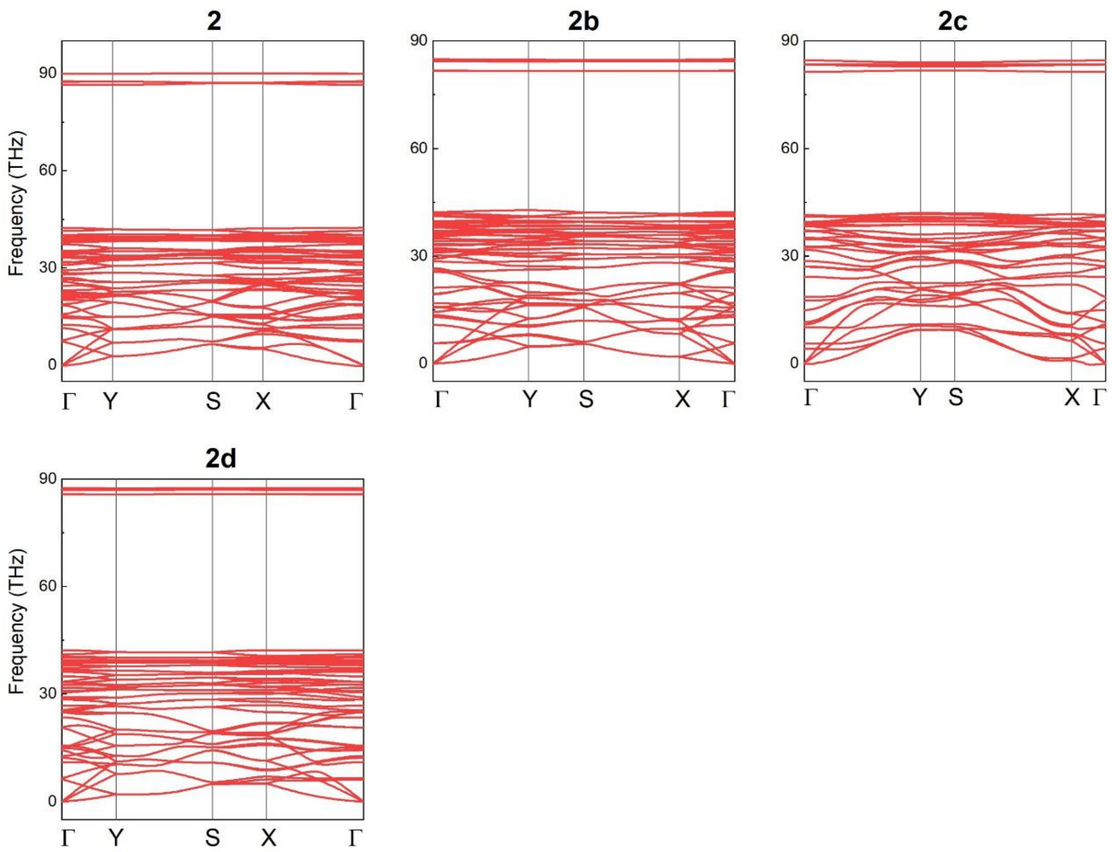

Figure S2 Phonon dispersion curves of 2D HCN structures of family **B**: **2** and **2b-d** phases

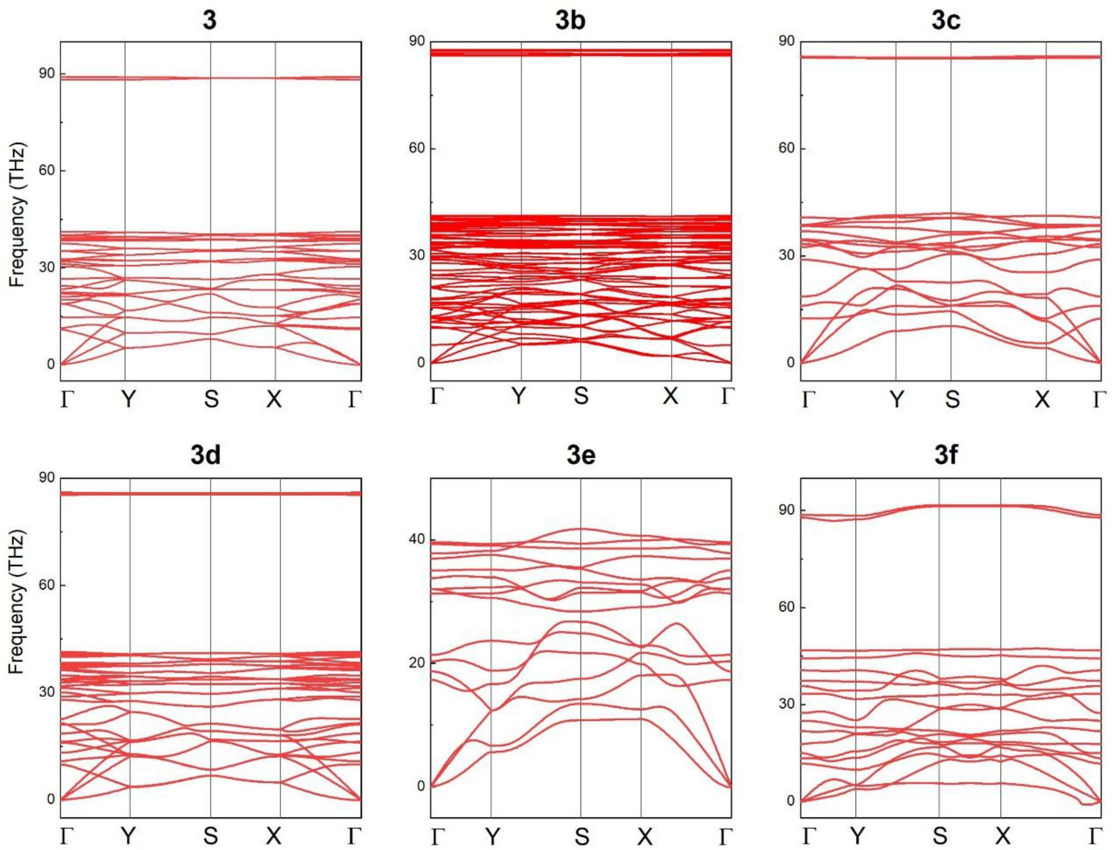

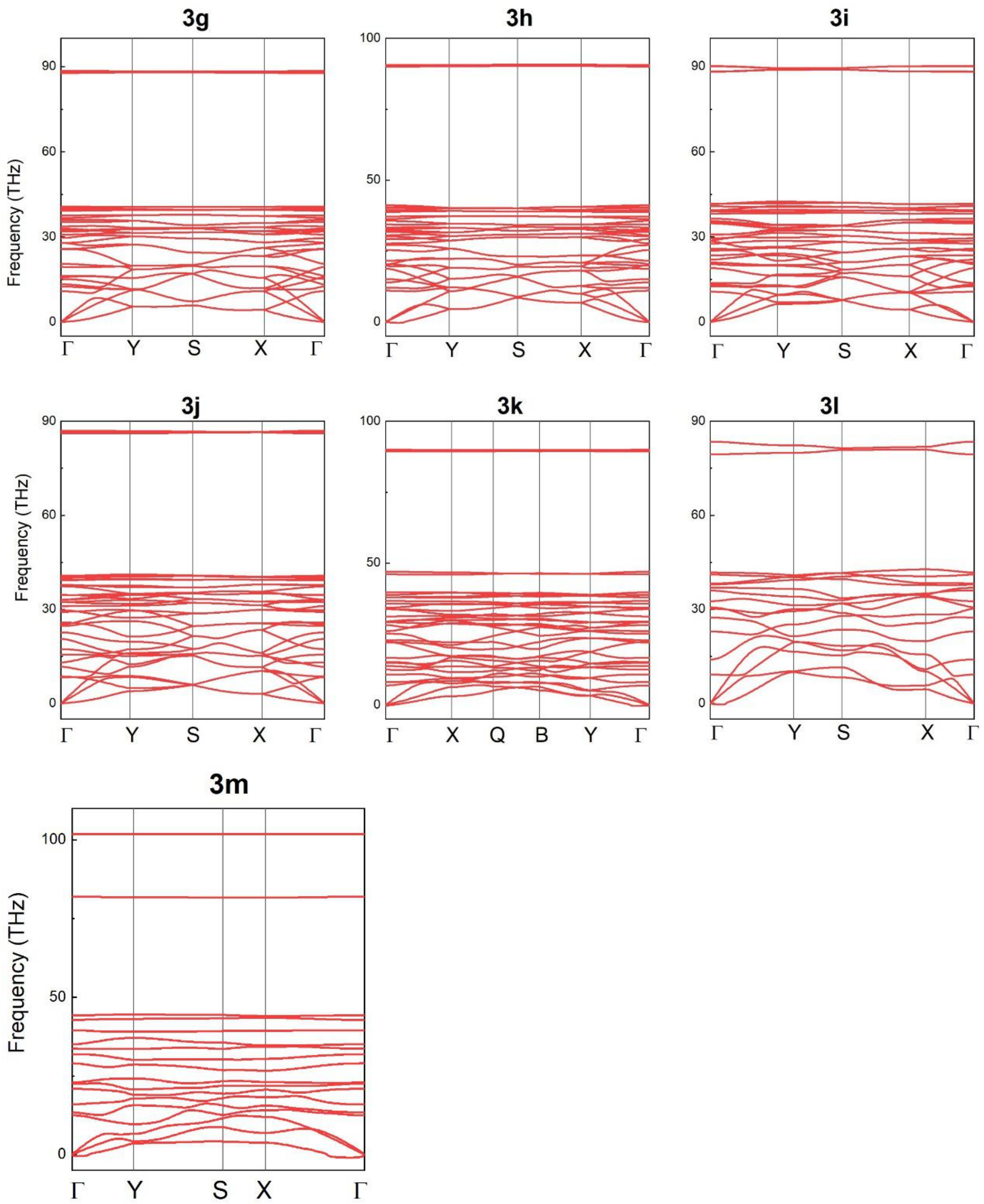

Figure S3 Phonon dispersion curves of 2D HCN structures of family **C**: **3** and **3b-m** phases

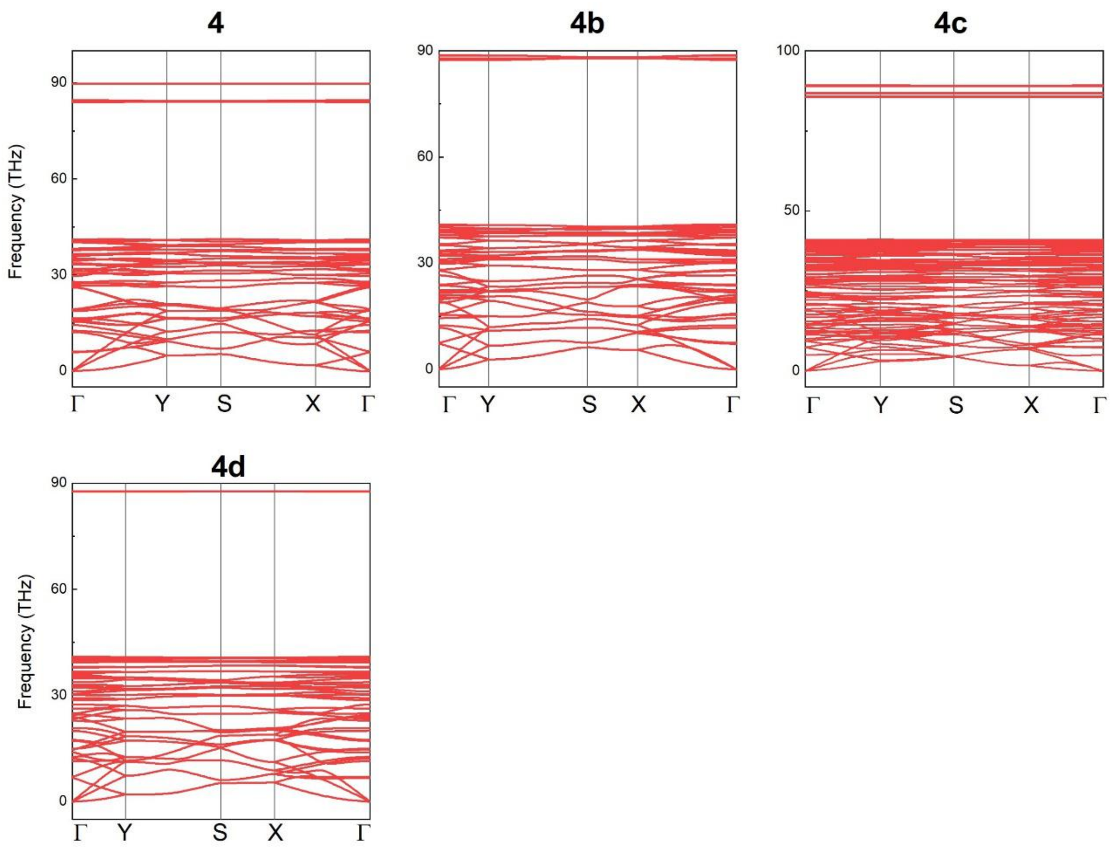

Figure S4 Phonon dispersion curves of 2D HCN structures of family **D**: **4** and **4b-d** phases

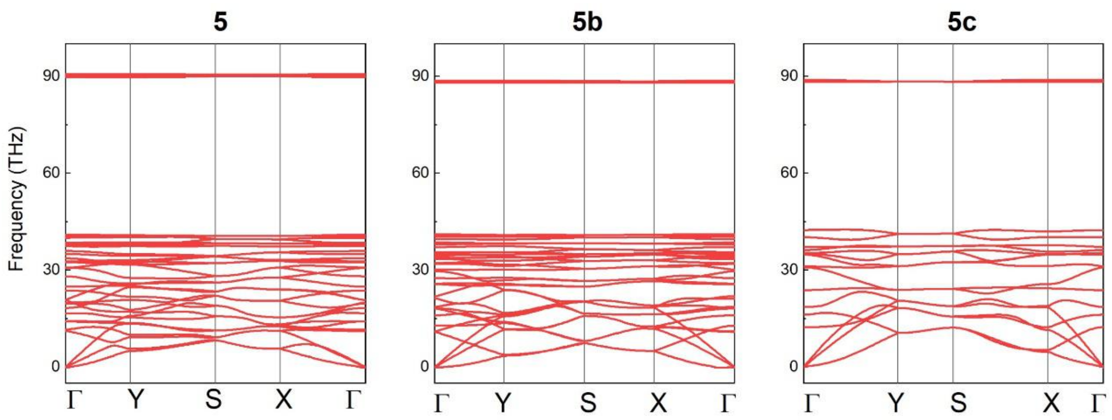

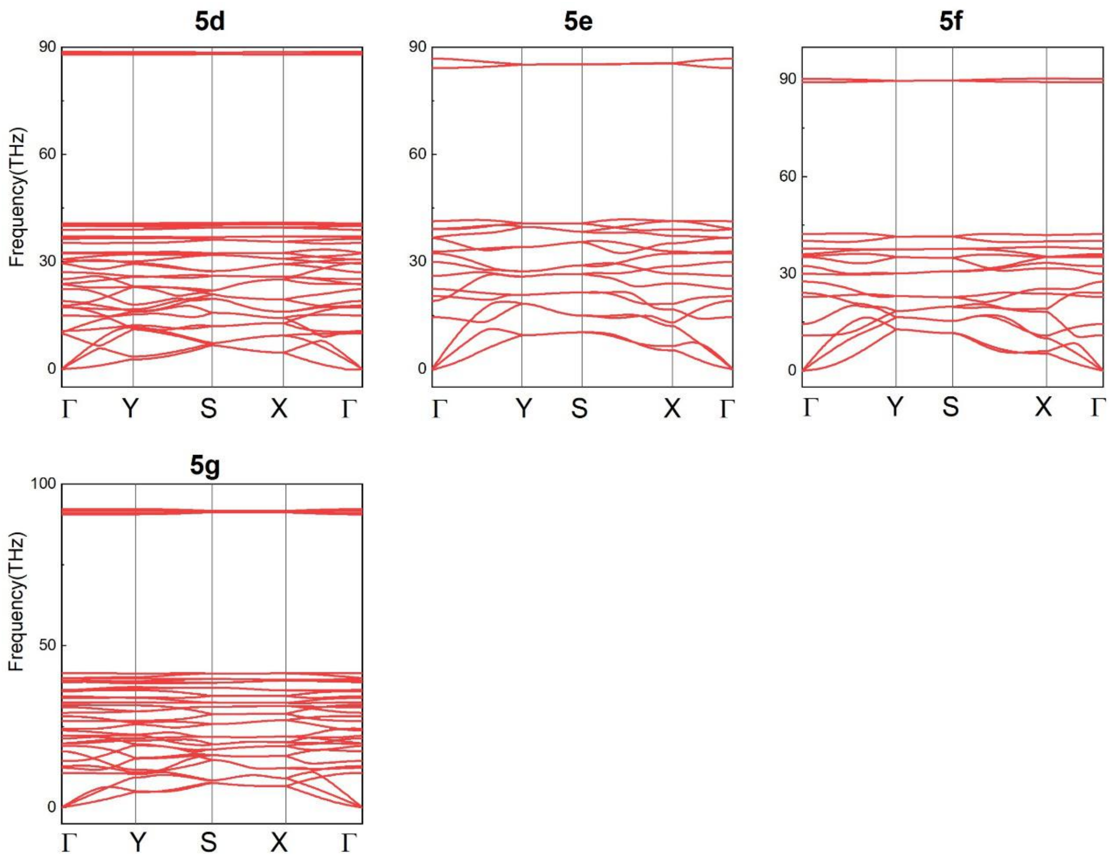

Figure S5 Phonon dispersion curves of 2D HCN structures of family **E**: **5** and **5b-g** phases

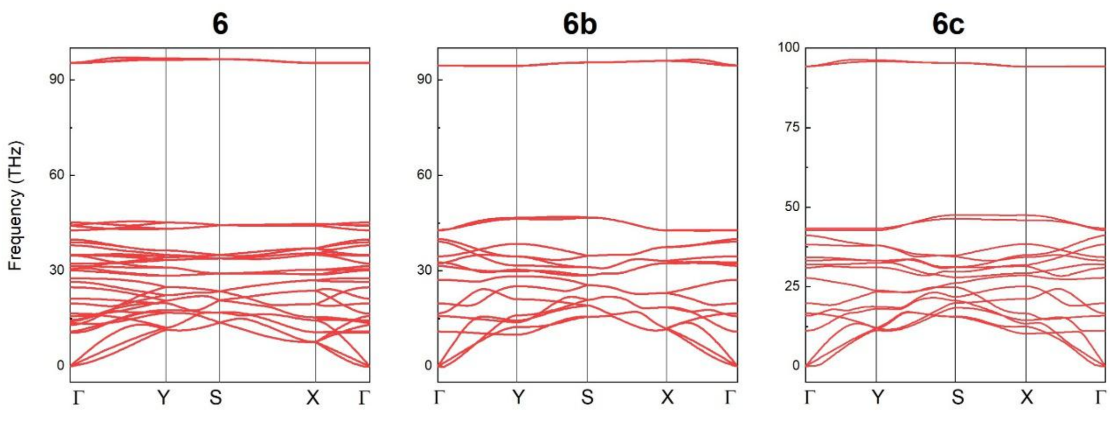

Figure S6 Phonon dispersion curves of 2D HNC structures of family **F**: **6**, and **6b-c** phases

S5 Structures of 2D HCN and HNC structures

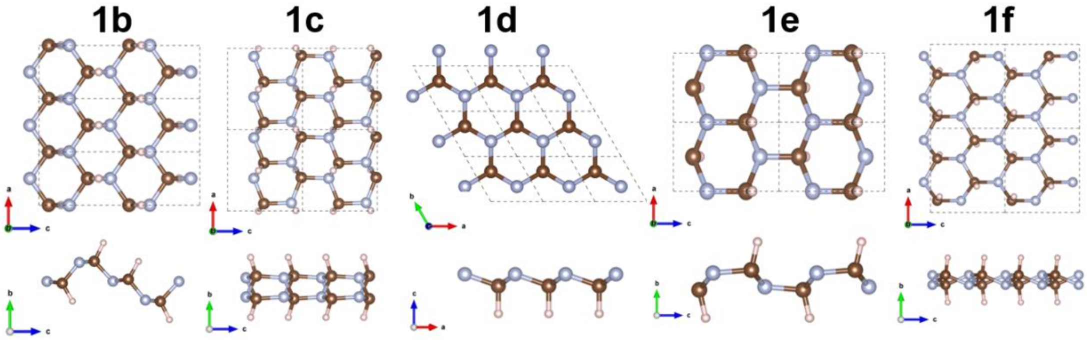

Figure S7 Structure configurations of 2D HCN structures of family **A**: **1b-e** phases

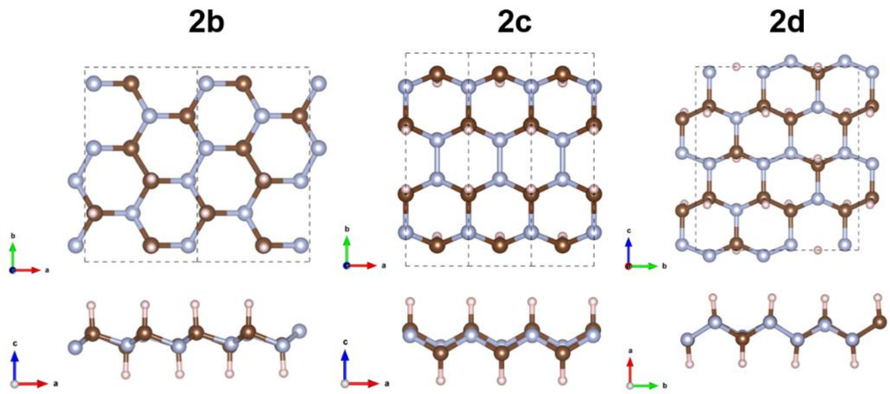

Figure S8 Structure configurations of 2D HCN structures of family **B**: **2b-d** phases

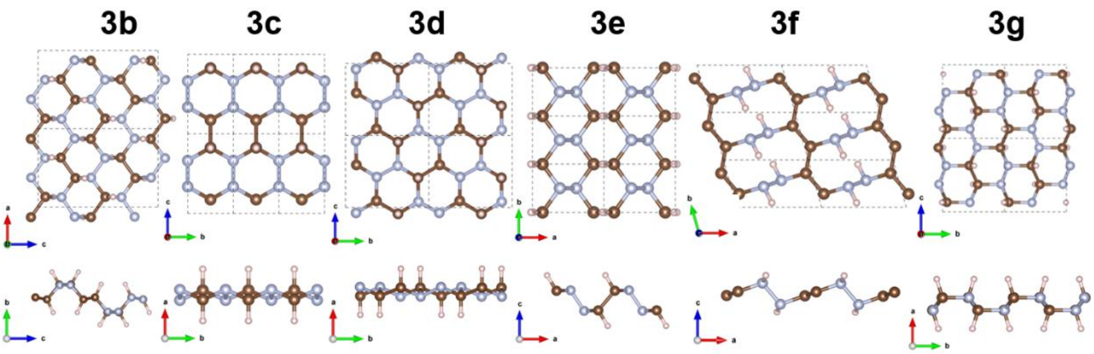

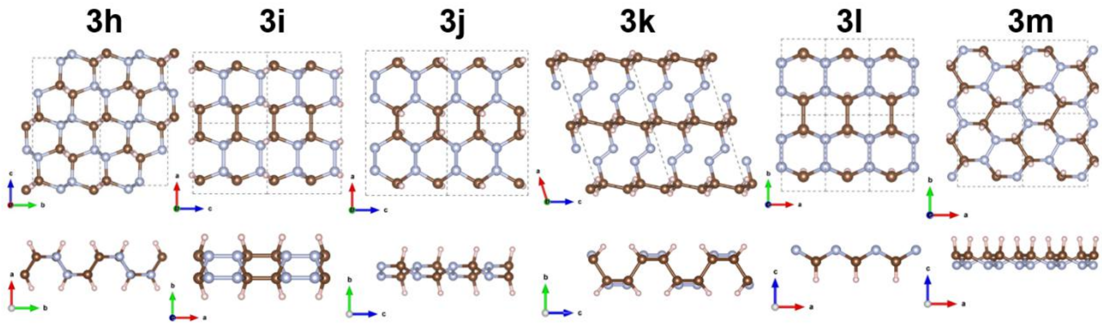

Figure S9 Structure configurations of 2D HCN structures of family **C**: **3b-m** phases

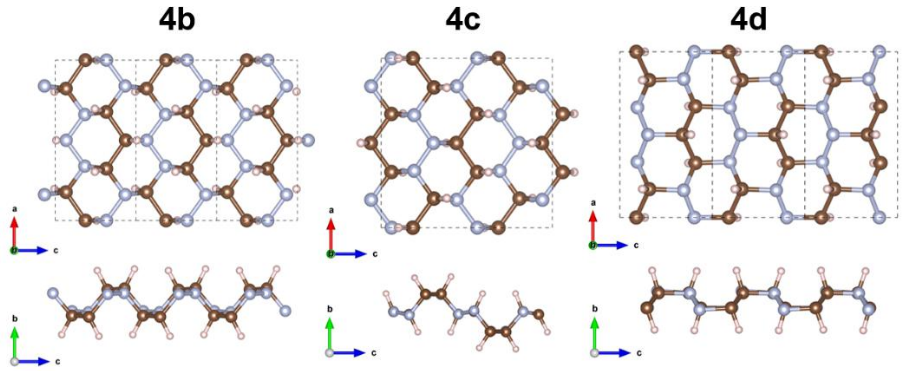

Figure S10 Structure configurations of 2D HCN structures of family **D**: **4b-d** phases

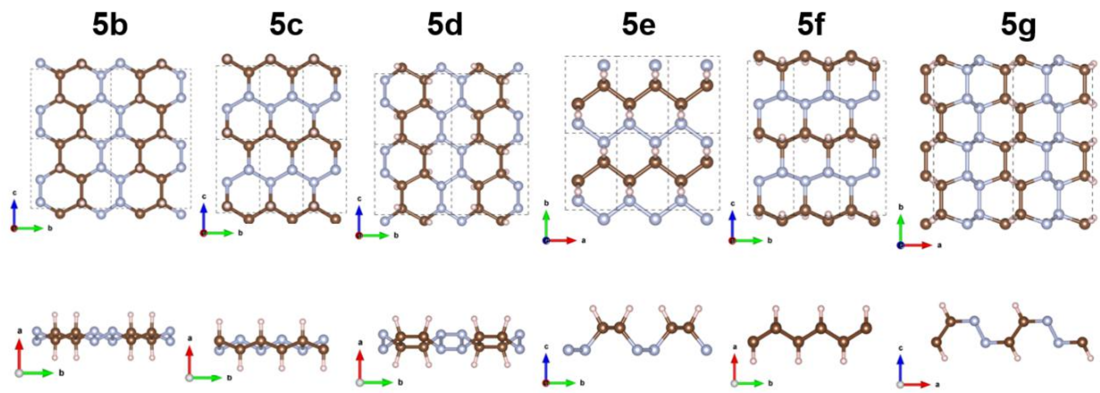

Figure S11 Structure configurations of 2D HCN structures of family **E**: **5b-g** phases

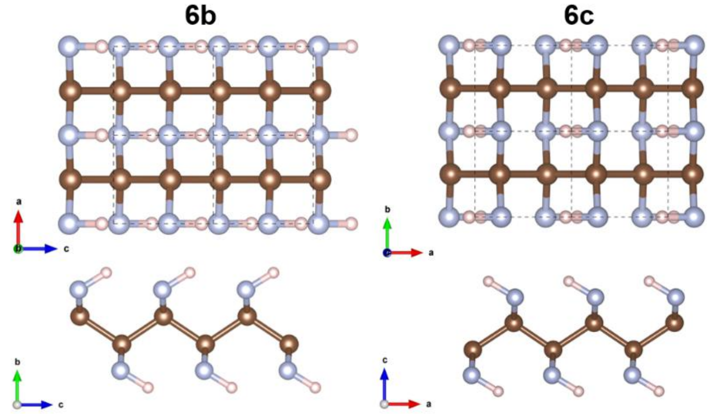

Figure S12 Structure configurations of 2D HNC structures of family **F**: **6b**, and **6c** phases

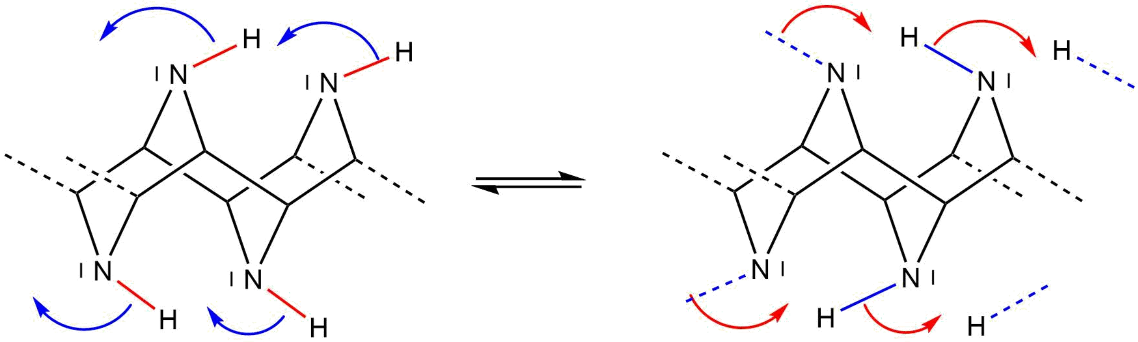

Figure S13 Schematic diagram of proton migration in 2D HNC structures

S6 Phase viabilities of 2D HCN and HNC structures

S6.1 Mechanical stabilities of 2D HCN and HNC structures

Table S4 Calculated elastic constants (N/m) of 2D HCN and HNC structures at the PBE level of theory

Phase	C_{11}	C_{12}	C_{22}	C_{33}
1 *Pmn*2$_1$ HCN	109.0	39.9	353.2	101.9
2 *Pma*2 HCN	334.1	39.3	118.4	97.9
3 *P*2$_1$2$_1$2 HCN	120.1	24.7	335.5	96.8
4 *Cm* HCN	282.4	32.5	291.3	132.8
5 *P*222$_1$ HCN	111.3	43.5	337.1	88.3
6 *Pbcm* HNC	260.2	11.5	446.3	77.9

S6.2 Thermal stabilities of 2D HCN and HNC structures

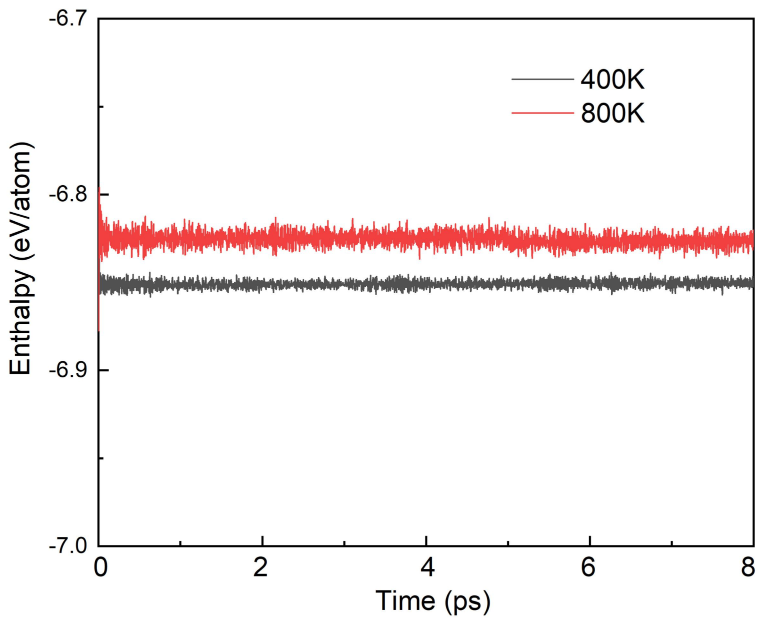

Figure S14 Energy fluctuations of 2D **1** *Pmn*2$_1$ HCN during the AIMD simulations at specific temperatures, T = 400K and 800K

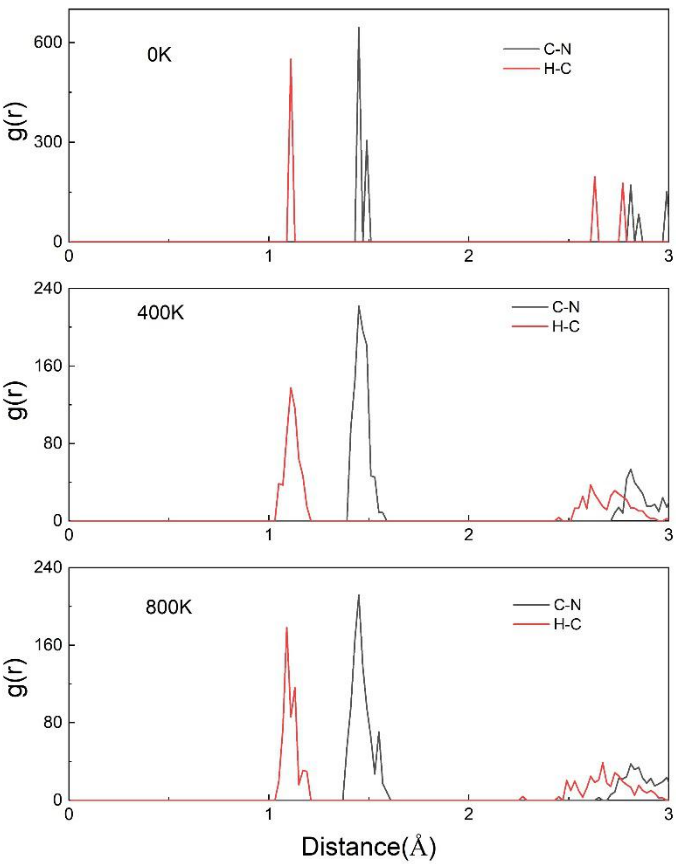

Figure S15 Radial distribution functions (RDF) $g(r)$ for the C-N, and C-H distances observed during AIMD simulations at 400K and 800K in 2D **1** $Pmn2_1$ HCN

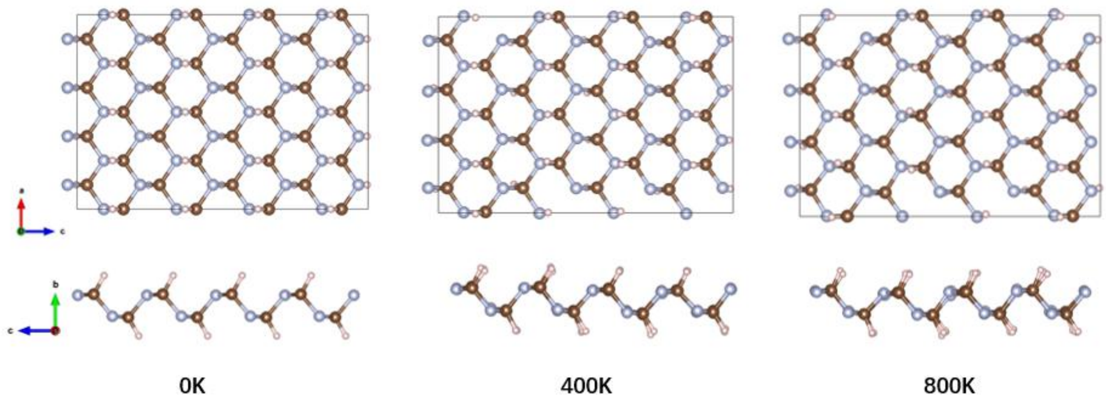

Figure S16 Snapshots of 2D **1** $Pmn2_1$ HCN supercell (4×4) at ambient pressure at the end of 8 ps

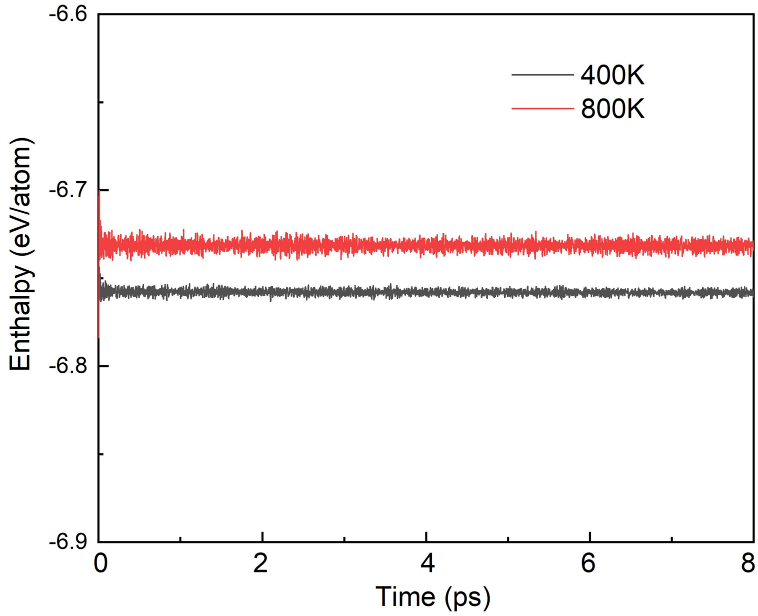

Figure S17 Energy fluctuations of 2D **2** *Pma*2 HCN during the AIMD simulations at specific temperatures, T = 400K and 800K

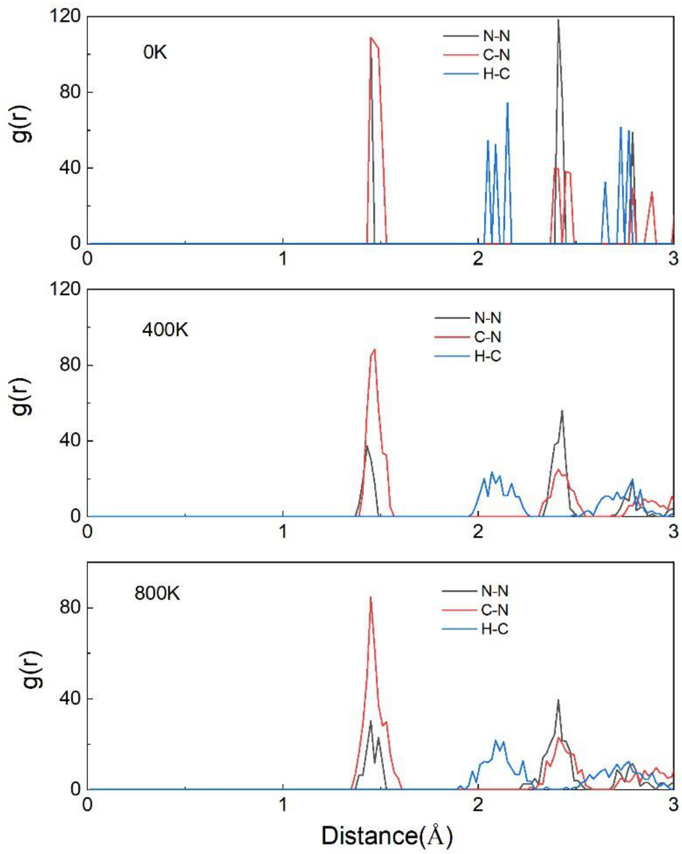

Figure S18 Radial distribution functions (RDF) $g(r)$ for the C-N, C-H, and N-N distances observed during AIMD simulations at 400K and 800K in 2D **2** *Pma*2 HCN

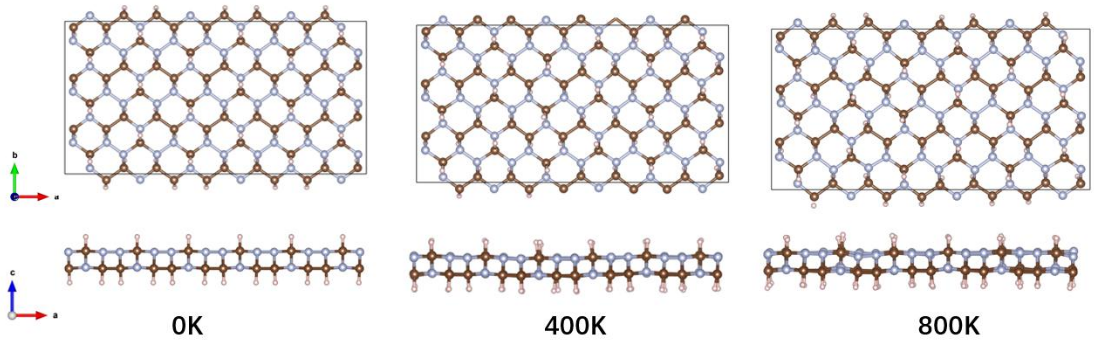

Figure S19 Snapshots of 2D **2** *Pma*2 HCN supercell (4×4) at ambient pressure at the end of 8 ps

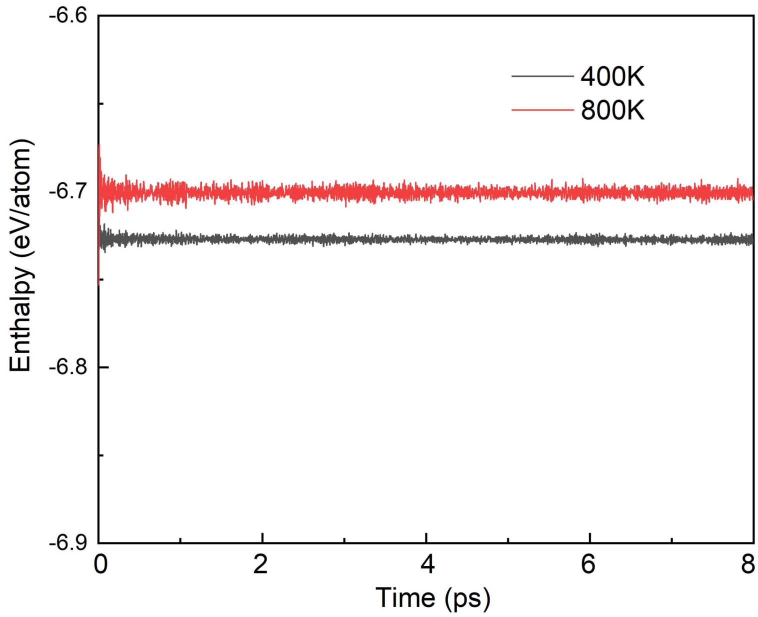

Figure S20 Energy fluctuations of 2D **3** $P2_12_12$ HCN during the AIMD simulations at specific temperatures, T = 400K and 800K

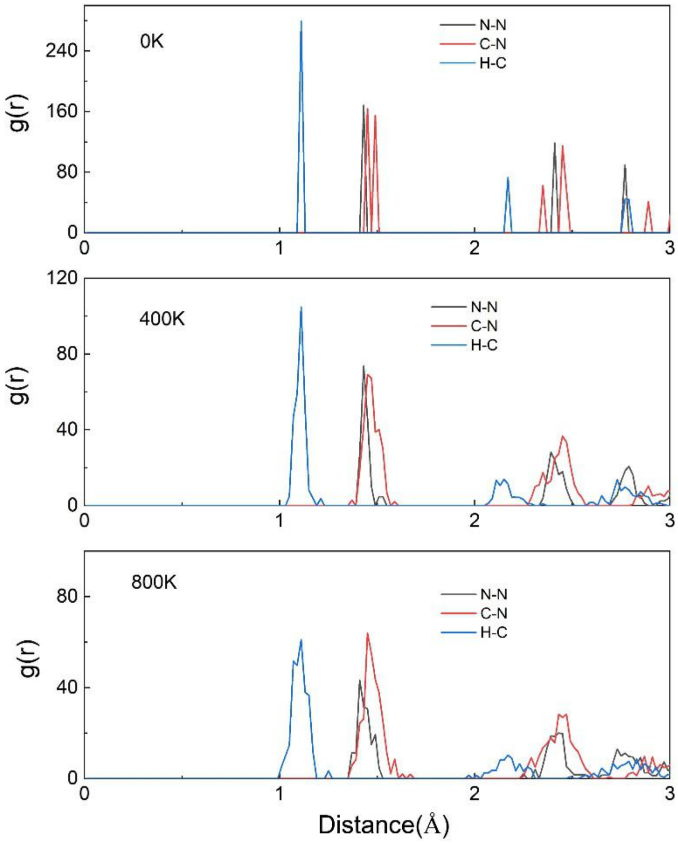

Figure S21 Radial distribution functions (RDF) $g(r)$ for the C-N, C-H, and N-N distances observed during AIMD simulations at 400K and 800K in 2D **3** $P2_12_12$ HCN

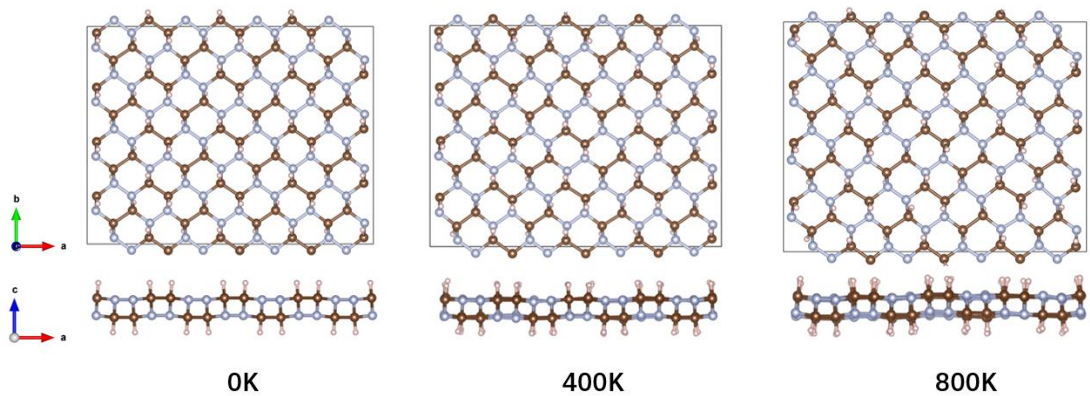

Figure S22 Snapshots of the 2D **3** $P2_12_12$ HCN supercell (4×4) at ambient pressure at the end of 8 ps

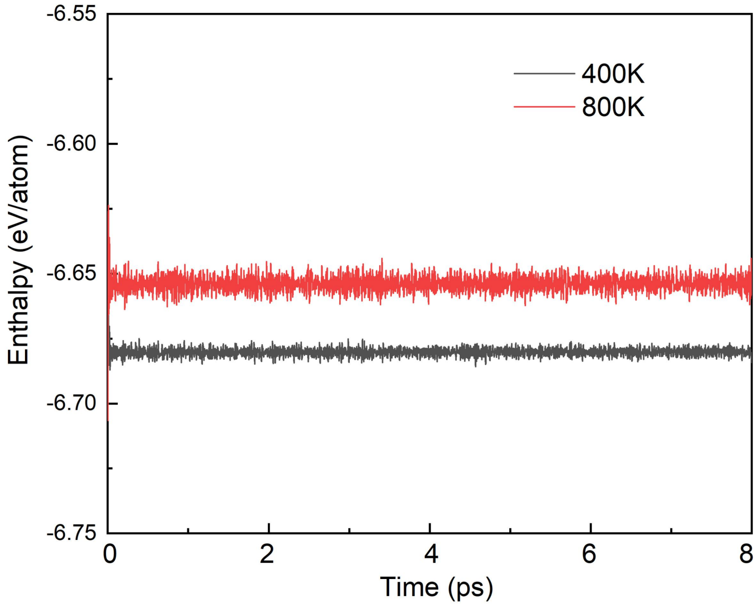

Figure S23 Energy fluctuations of 2D **4** *Cm* HCN during the AIMD simulations at specific temperatures, T = 400K and 800K

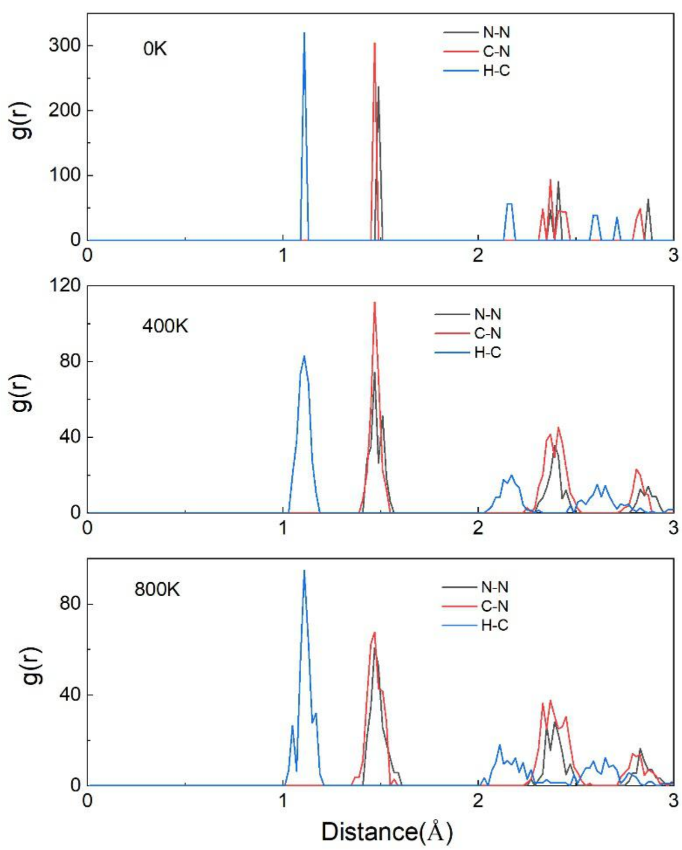

Figure S24 Radial distribution functions (RDF) $g(r)$ for the C-N, C-H, and N-N distances observed during AIMD simulations at 400K and 800K in 2D **4** *Cm* HCN

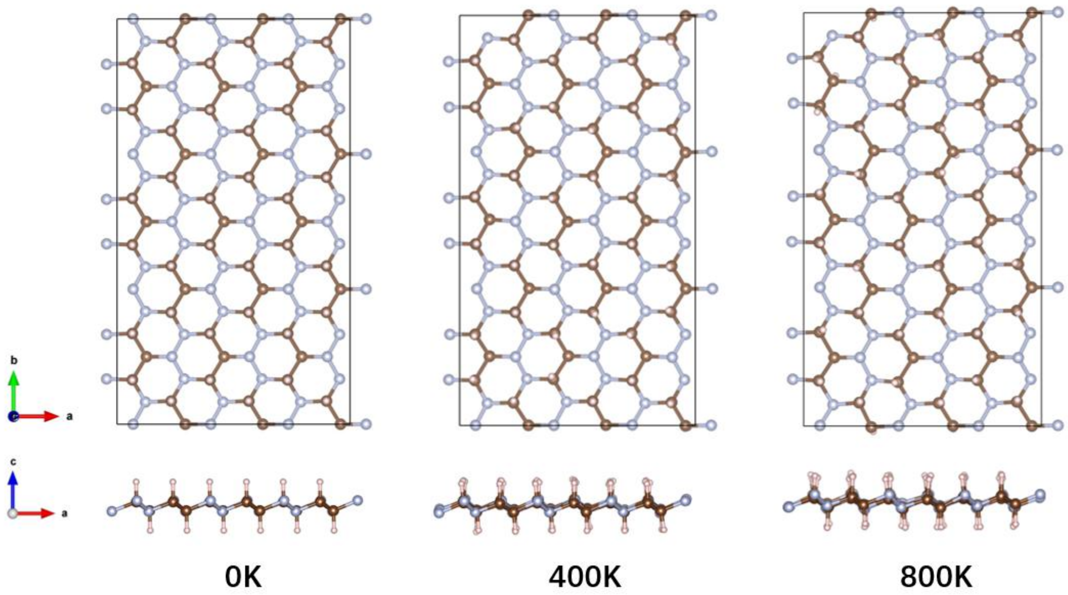

Figure S25 Snapshots of the 2D **4** *Cm* HCN supercell (3×3) at ambient pressure at the end of 8 ps

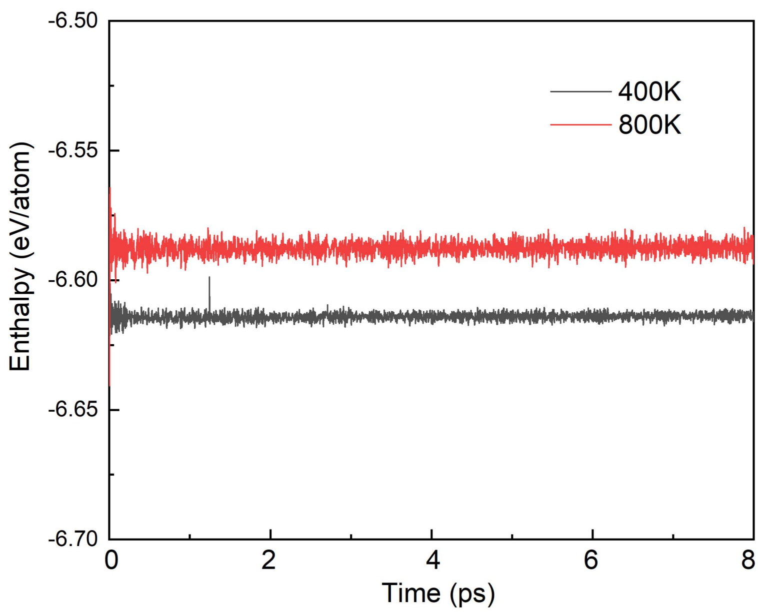

Figure S26 Energy fluctuations of 2D **5** $P222_1$ HCN during the AIMD simulations at specific temperatures, T = 400K and 800K

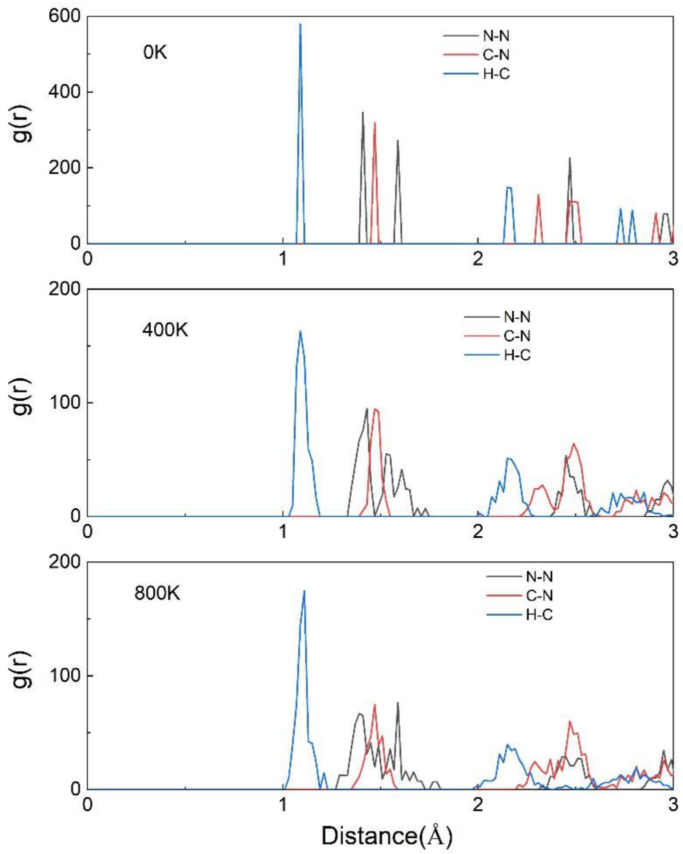

Figure S27 Radial distribution functions (RDF) $g(r)$ for the C-N, C-H, and N-N distances observed during AIMD simulations at 400K and 800K in 2D **5** $P222_1$ HCN

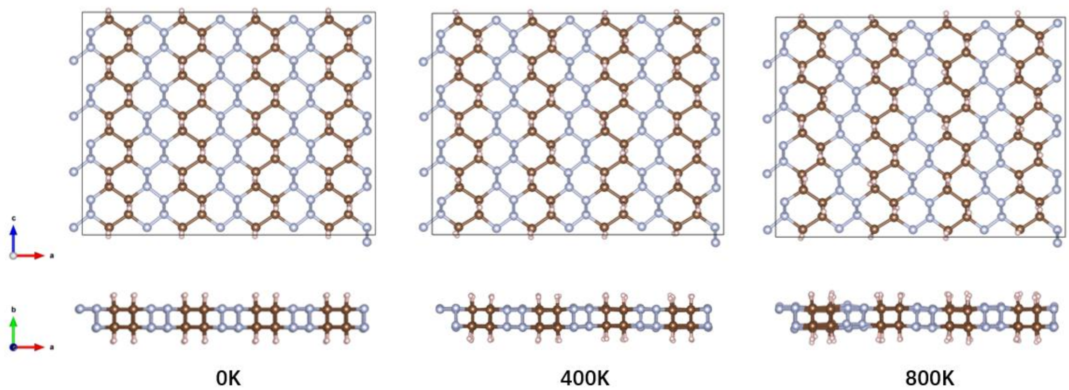

Figure S28 Snapshots of the 2D **5** $P222_1$ HCN supercell (4×4) at ambient pressure at the end of 8 *ps*

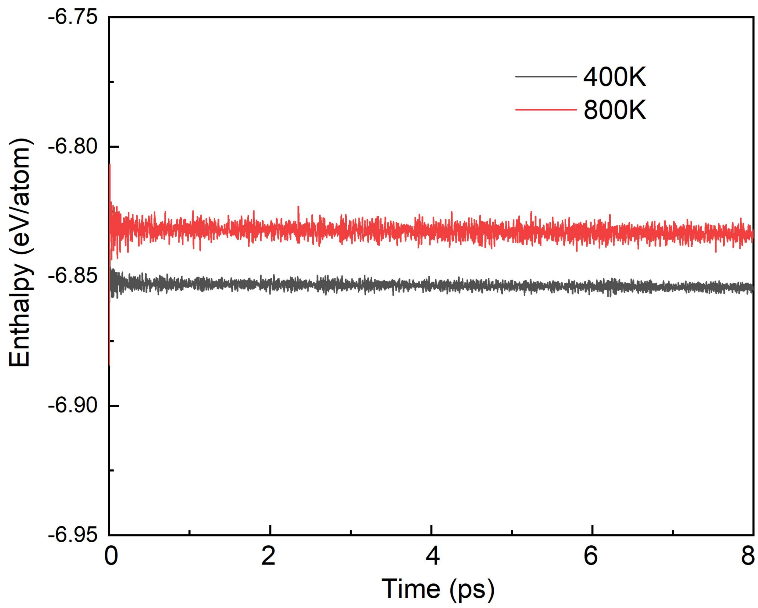

Figure S29 Energy fluctuations of 2D **6** *Pbcm* HNC during the AIMD simulations at specific temperatures, T = 400K and 800K

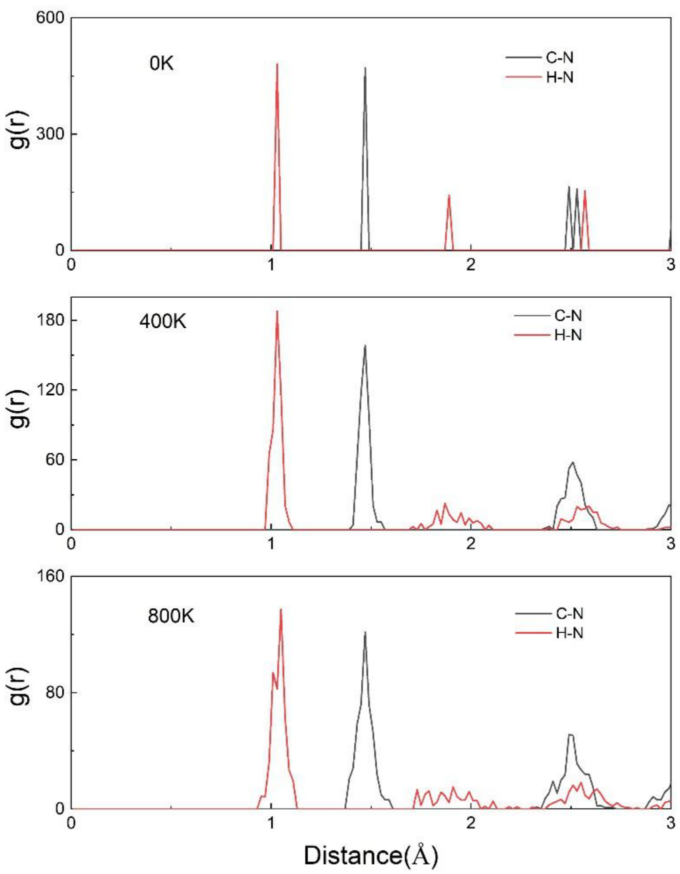

Figure S30 Radial distribution functions (RDF) $g(r)$ for the C-N, C-H, and N-N distances observed during AIMD simulations at 400K and 800K in 2D **6** *Pbcm* HNC

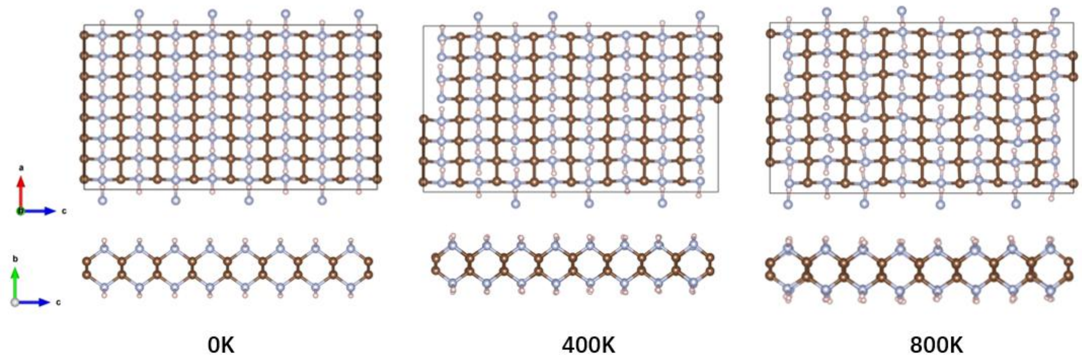

Figure S31 Snapshots of the 2D **6** *Pbcm* HNC supercell (4×4) at ambient pressure at the end of 8 ps

S7 Electronic properties of 2D HCN and HNC structures

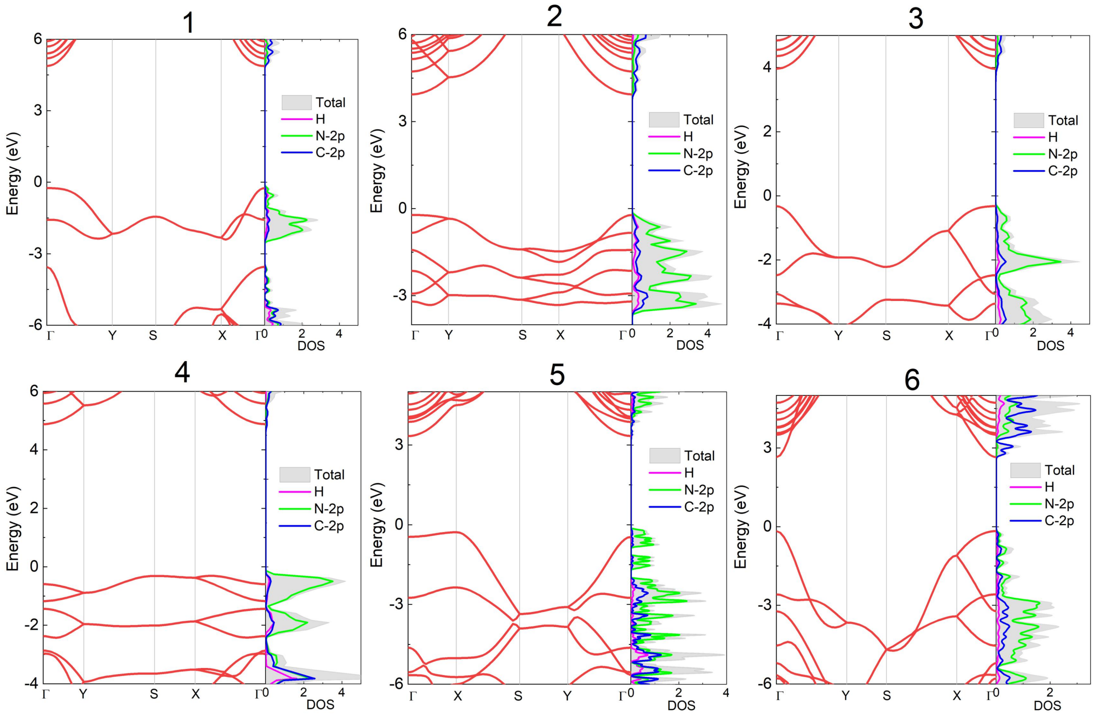

Figure S32 Calculated band structures and DOS (at the HSE06//PBE level of theory) of 2D HCN and HNC structures **1-6**: **1** *Pmn*2$_1$ HCN, **2** *Pma*2 HCN, **3** *P*2$_1$2$_1$2 HCN, **4** *Cm* HCN, **5** *P*222$_1$ HCN, and **6** *Pbcm* HNC. The Fermi energy is set to zero.

Table S5 Calculated energy band gaps of all 37 2D HCN and HNC structures at the GGA PBE and HSE06//PBE levels of theory

family	Phase	Z	Space Group	Band gap (eV)	
				PBE	HSE06//PBE
A	**1**	2	*Pmn*2$_1$	3.9	5.1
	1b	4	*Pmc*2$_1$	4.5	5.7
	1c	4	*Pca*2$_1$	3.7	4.5
	1d	1	*P*3*m*1	4.7	5.8
	1e	2	*Pmn*2$_1$	4.2	5.3
	1f	12	*Pca*2$_1$	3.3	4.3
B	**2**	6	*Pma*2	3.0	4.2
	2b	6	*P*2$_1$/*m*	4.3	5.6
	2c	4	*Pmm*2	3.6	4.8

	2d	6	$P2_1/m$	3.4	4.6
C	**3**	4	$P2_12_12$	3.2	4.3
	3b	8	$P2/c$	3.7	5.0
	3c	2	$P2/m$	4.1	5.4
	3d	4	$P2_1/c$	4.2	5.5
	3e	2	$P2/m$	2.4	3.6
	3f	2	$P\text{-}1$	2.4	3.9
	3g	4	$P2_1/c$	3.3	4.6
	3h	4	$P2_1/c$	2.0	3.4
	3i	4	$Pmc2_1$	2.5	3.8
	3j	4	$Pcc2$	2.9	4.5
	3k	4	$P2/c$	2.3	3.4
	3l	2	$Pmm2$	2.2	3.3
	3m	4	$Pba2$	2.4	3.5
D	**4**	6	Cm	4.0	5.2
	4b	6	$Pmn2_1$	2.6	3.8
	4c	8	$Pmc2_1$	3.4	4.6
	4d	6	$Pmn2_1$	3.2	4.4
E	**5**	4	$P222_1$	2.6	3.6
	5b	4	$P2/c$	4.1	5.3
	5c	2	$P2_1/m$	3.0	4.4
	5d	4	$P222_1$	2.6	3.9
	5e	2	$Pma2$	1.7	2.9
	5f	2	$P2_1/m$	1.9	3.1
	5g	4	$P2_1/m$	1.8	3.0
F	**6**	4	$Pbcm$	1.5	2.8
	6b	4	$Pmc2_1$	1.9	3.1
	6c	2	$P2/m$	1.7 1.72[34]	3.0 3.03[36]

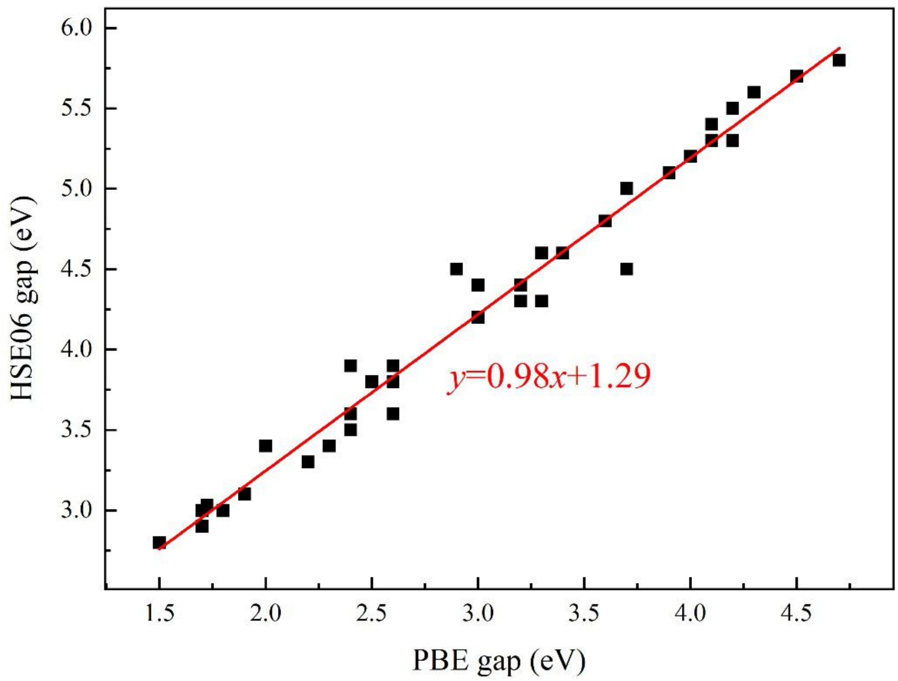

Figure S33 The fitting relationship between the HSE06 gaps and PBE gap of all 2D HCN structures.

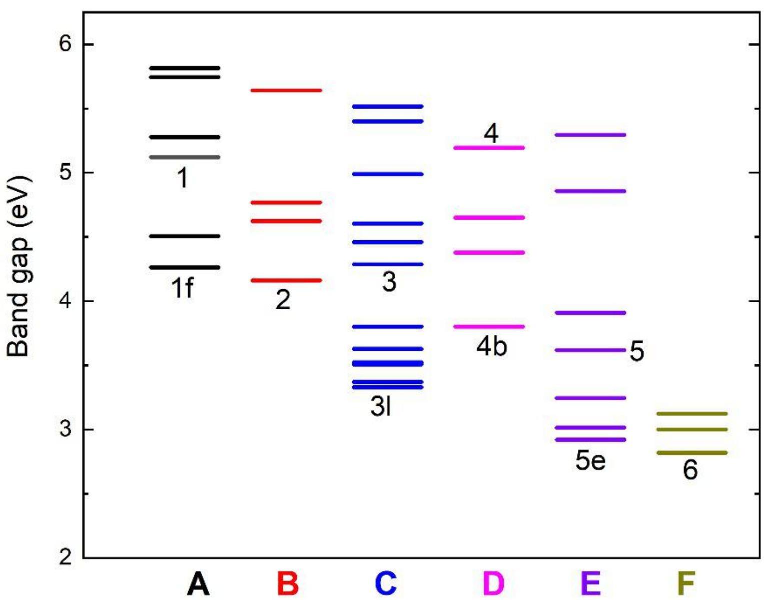

Figure S34 Energy band gaps of all 37 2D HCN and HNC structures at the HSE06//PBE level of theory. The structures with lowest band gaps in each topological family are indicated, as well as structures **1**-**6**.

Table S6 Calculated Manz bond orders of C-N, C-C, N-N, H-C, and H-N bonds in **1-6** 2D compounds at the PBE level of theory. The bond distances are indicated in the brackets.

phase	Bond order				
	C-N	C-C	N-N	H-C	H-N
1 *Pmn*2_1 HCN	0.96(1.45Å) 0.85(1.49Å)	-	-	0.74(1.11Å)	-
2 *Pma*2 HCN	1.00(1.44Å) 0.92(1.47Å) 0.88(1.49Å) 0.85(1.50Å)	0.83(1.51Å)	0.99(1.45Å)	0.76(1.10Å) 0.75(1.11Å)	-
3 *P*2_12_12 HCN	0.98(1.45Å) 0.88(1.49Å)	0.81(1.54Å)	1.01(1.43Å)	0.76(1.10Å)	-
4 *Cm* HCN	0.91(1.46Å) 0.90(1.47Å) 0.90(1.48Å)	0.82(1.52Å)	0.88(1.48Å)	0.74(1.10Å) 0.74(1.12Å)	-
5 *P*222_1 HCN	0.93(1.48Å)	0.86(1.52Å) 0.84(1.53Å)	1.11(1.40Å) 0.70(1.59Å)	0.75(1.10Å)	-
6 *Pbcm* HNC	0.93(1.47Å)	0.64(1.62Å)	-	-	0.76(1.03Å)

S8 Young's modulus and Poisson's ratio of 2D HCN and HNC structures

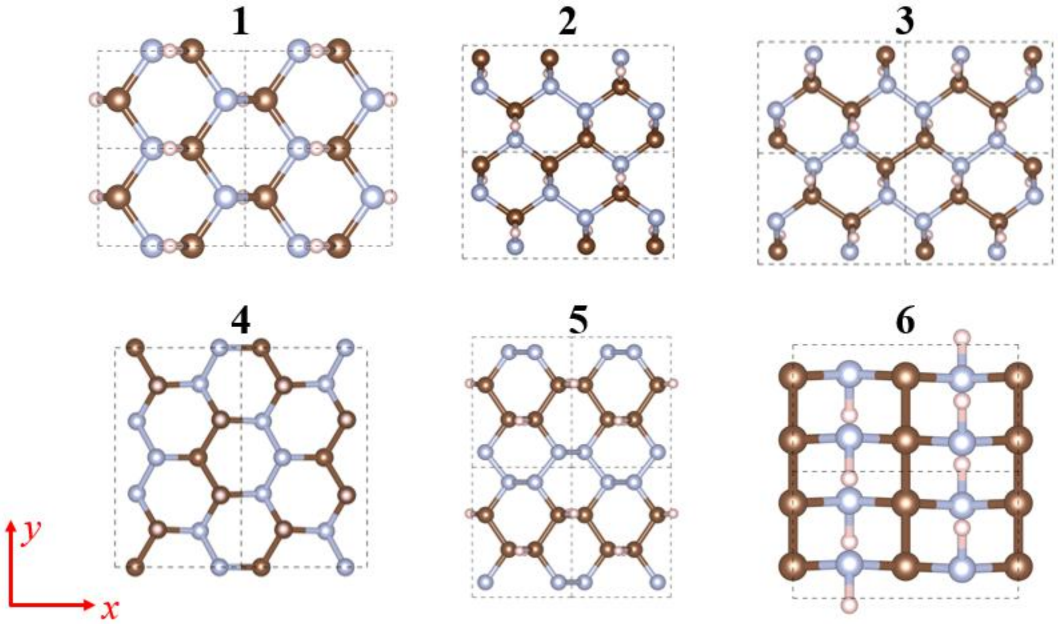

Figure S35 Representation of the chosen crystal models for the evaluation of mechanical properties for 2D **1** *Pmn*2_1 HCN (x=3.581 Å, y=2.380 Å), **2** *Pma*2 HCN (x=7.169 Å, y=3.614 Å), **3** $P2_12_12$ HCN (x=4.782 Å, y=3.620 Å), **4** *Cm* HCN (x=4.133 Å, y=7.192 Å), **5** $P222_1$ HCN (x=3.623 Å, y=4.779 Å), and **6** *Pbcm* HNC (x=2.687 Å, y=4.774 Å). The x direction is along c axis in 2D **1** and **5**, along a axis in 2D **2**, **3**, and **4**, and along b axis in 2D **6**.

Table S7 Comparison of crystallographic parameters (a, b), and in-plane Young's modulus Y_{12} and Y_{21} of 2D $P\bar{3}m1$ silicene (Si), *Pmna* black phosphorene (BP) and $P\bar{6}m2$ molybdenum disulfide (MoS_2). The calculation methods of in-plane Young's modulus can be referred to Section 1.4 and computational models are depicted in Figure S35.

phase	Lattice parameters (Å)	Young's modulus (N/m)
2D Si	a=6.701 b=3.866 a=6.703[37], 6.694[38] b=3.870[37],3.385[38]	Y_{12}=64.24 Y_{21}=62.79 Y_{12}=60.06~66.72[37], 63.8[38] Y_{21}=61.8~53.51[37]
2D BP	a=4.623	Y_{12}=22.939

	b=3.290 a = 4.62[39], 4.62[40] b = 3.01[39], 3.30[40]	Y_{21}=98.387 Y_{12}=21.348[39] Y_{21}=91.077[39]
2D MoS_2	a= 3.184 a=3.19[41, 42]	Y_{12}=Y_{21}=122.530 Y_{12}=Y_{21}=123.916[39], 122.123[42]

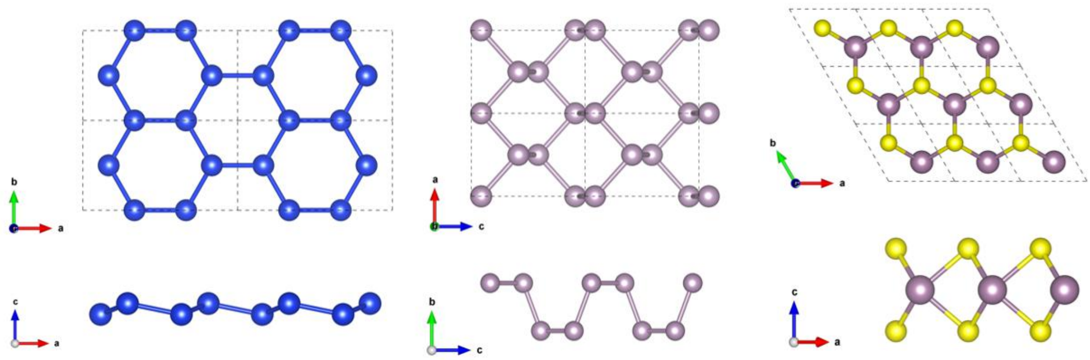

$P\bar{3}m1$ Si $Pmna$ BP $P\bar{6}m2$ MoS_2

Figure S36 Crystal structure views of 2D $P\bar{3}m1$ Si, *Pmna* BP, and $P\bar{6}m2$ MoS_2

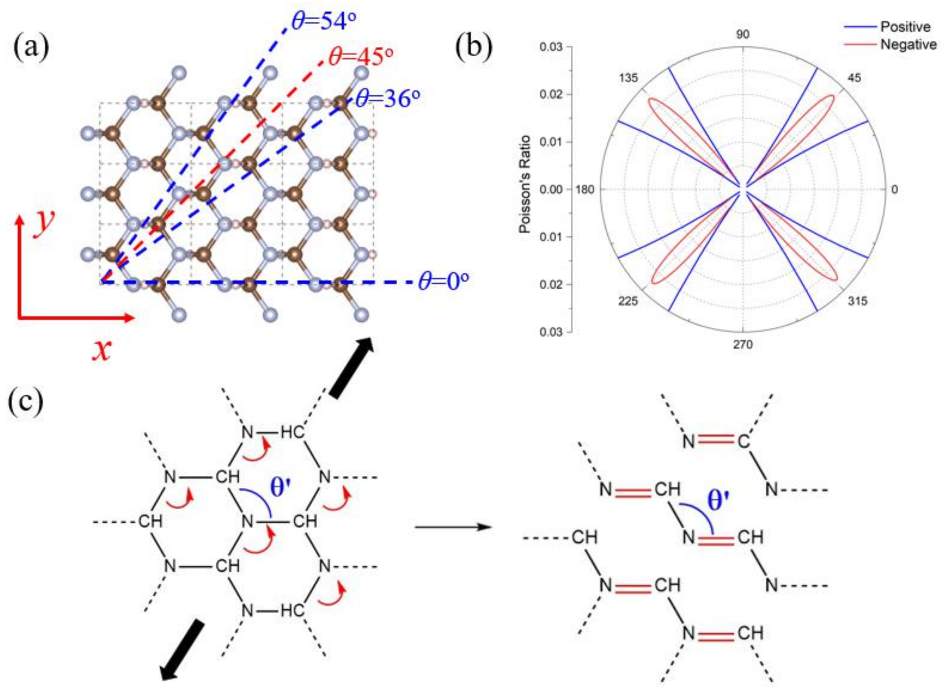

Figure S37 Negative Poisson's ratio of 2D **1** *Pmn*2$_1$ HCN: (a) Crystal structure view; (b) In-plane Poisson's ratio of 2D **1** *Pmn*2$_1$ HCN as a function of the angle θ at the PBE level of theory; (c) Mechanism of the negative Poission's ratio. Negative Poisson's ratios are found along the angle range of 36°<θ<54°.

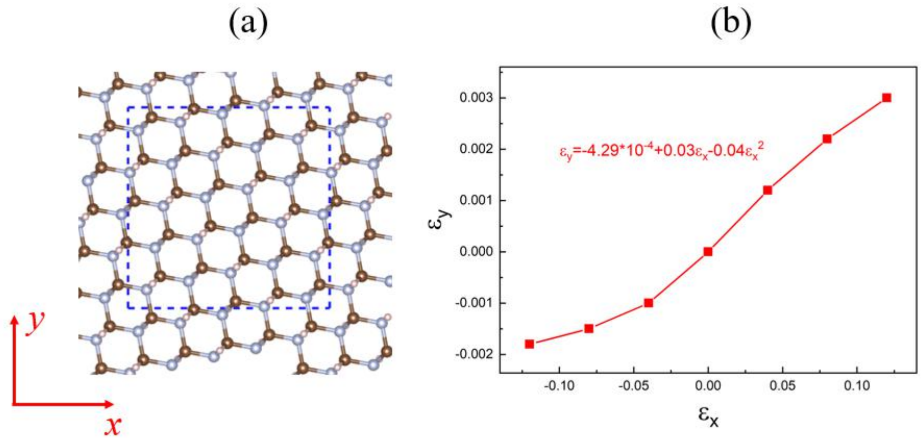

Figure S38 Negative Poisson's ratio of 2D **1** *Pmn*2$_1$ HCN along the θ=45°: (a) Computational model of rectangular lattice (x=y=10.182 Å, 72 atoms); (b) Strain response along the y direction (ε_x) vs the strain along x direction(ε_x). In (a), the unit cell is indicated in blue dash line. In (b), the tensile (compressive) strain was represented using the positive (negative) sign. The calculated Poisson's ratio using quadratic curve fitting is $\nu = -\partial\varepsilon_y/\partial\varepsilon_x = -0.03$.

S9 Strain effect on the electronic properties of 2D HCN

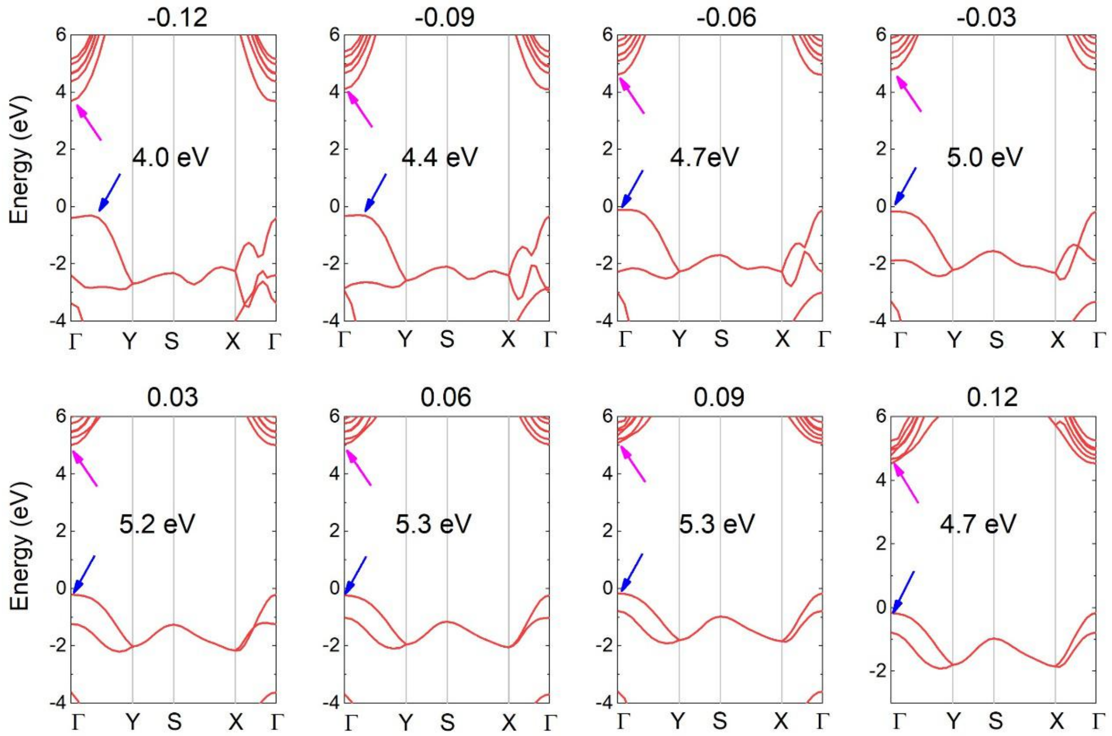

Figure S39 Calculated band structures of 2D **1** $Pmn2_1$ HCN under various strains at the HSE06//PBE level of theory. The strain is defined as $\Delta=(l'-l_0)/l_0$, in which l' is the strained lattice and l_0 is the equivalent lattice. Then, the compressive and tensile strains are indicated by negative and positive signs, respectively.

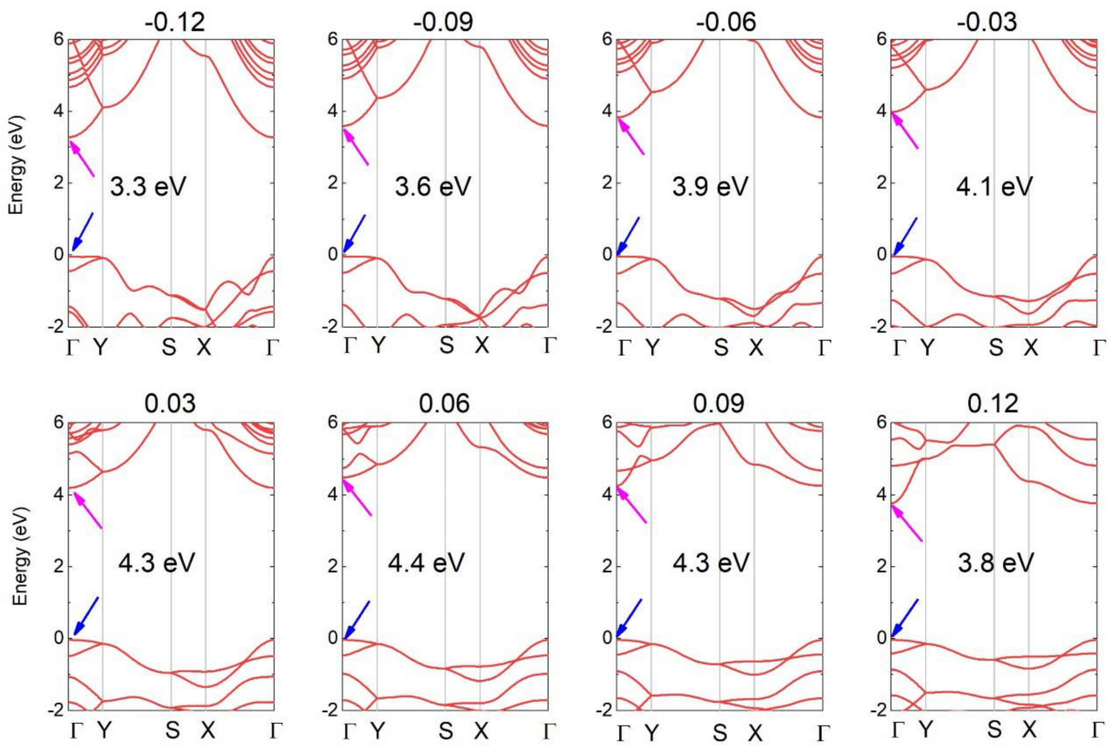

Figure S40 Calculated band structures of 2D **2** *Pma*2 HCN under various strains at the HSE06//PBE level of theory.

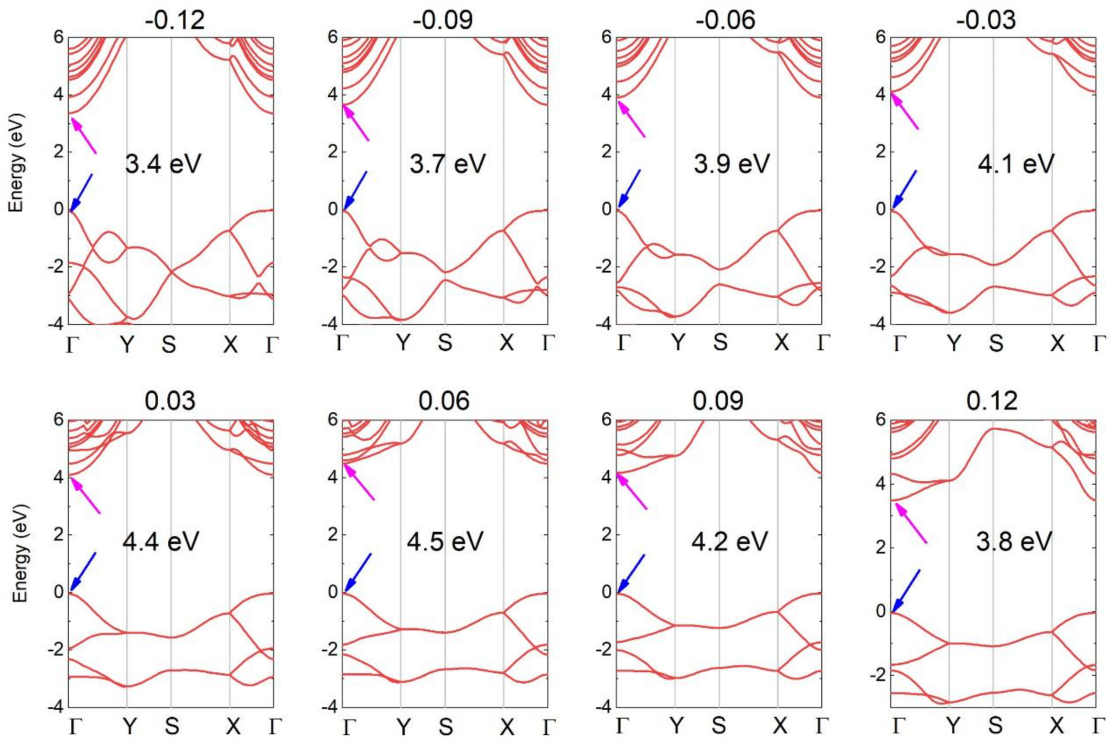

Figure S41 Calculated band structures of 2D **3** $P2_12_12$ HCN under various strains at the HSE06//PBE level of theory.

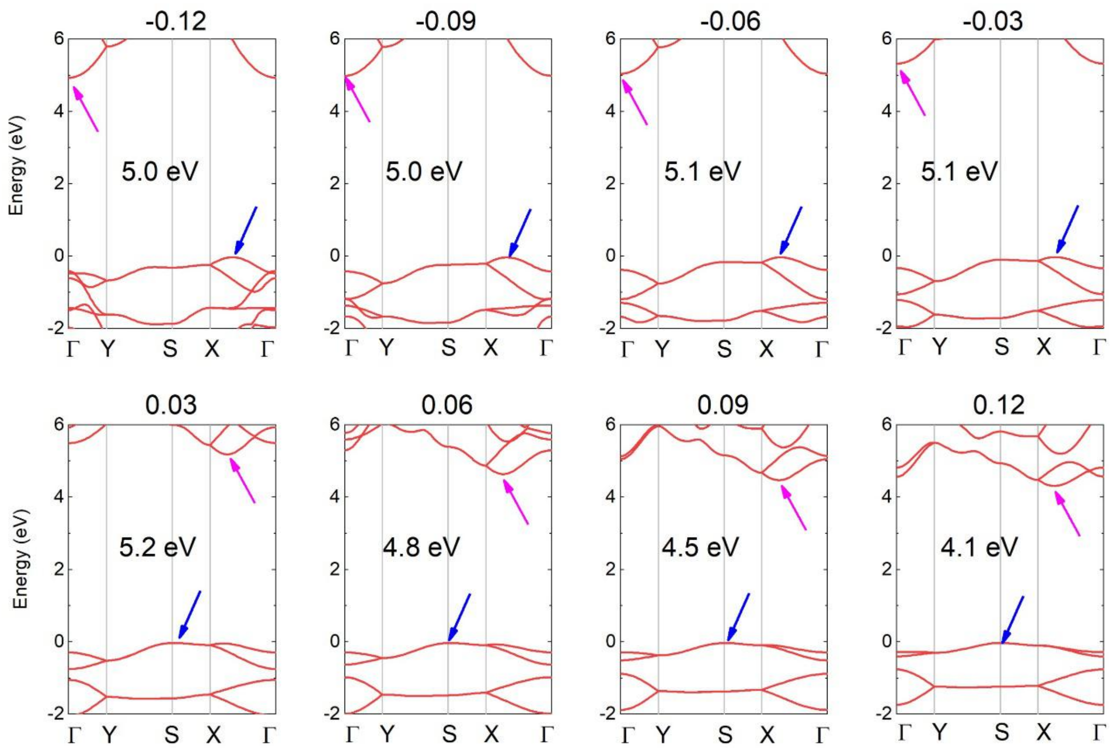

Figure S42 Calculated band structures of 2D **4** *Cm* HCN under various strains at the HSE06//PBE level of theory.

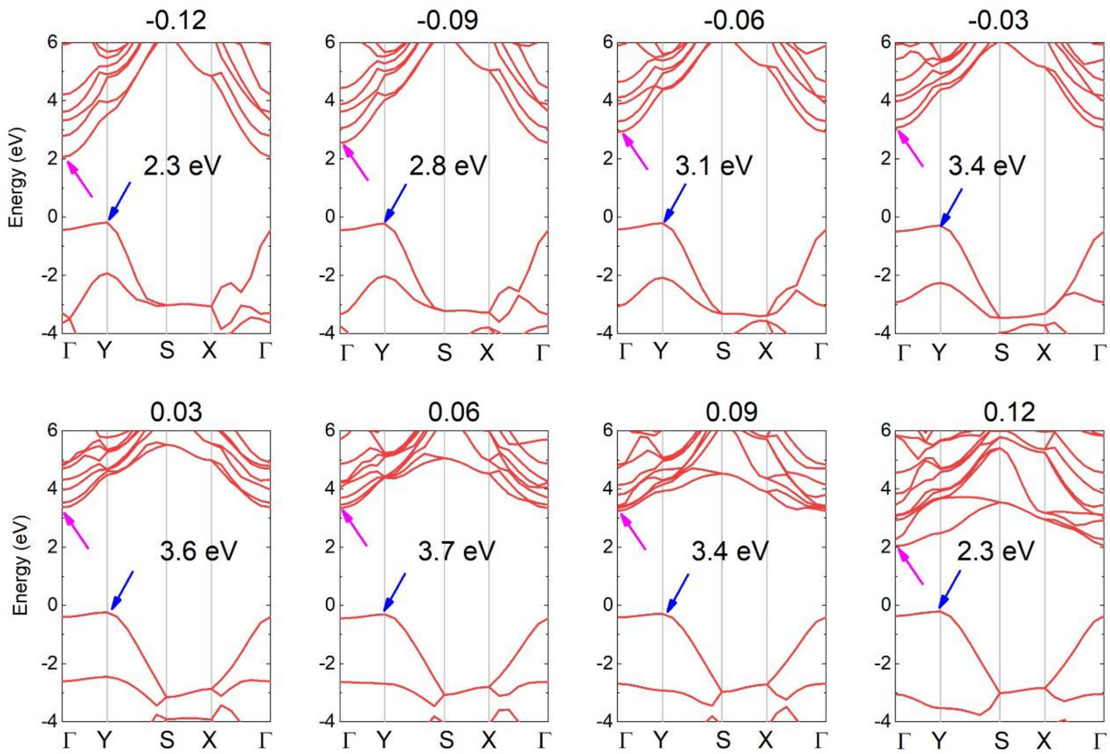

Figure S43 Calculated band structures of 2D **5** $P222_1$ HCN under various strains at the HSE06//PBE level of theory.

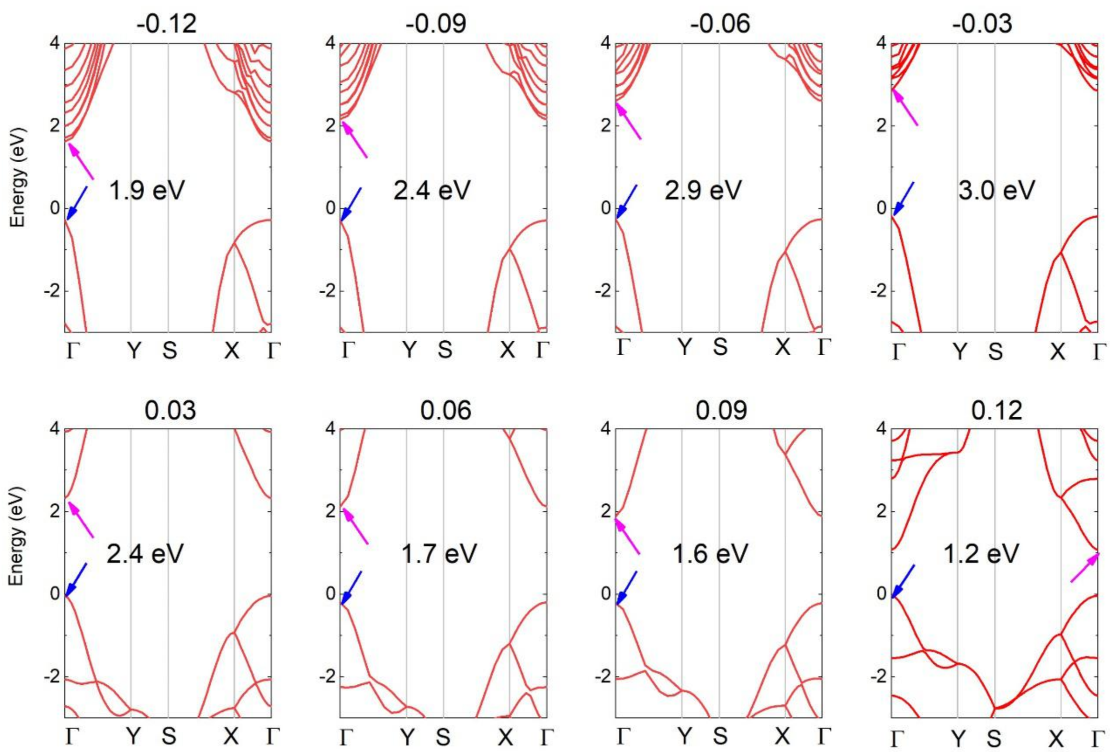

Figure S44 Calculated band structures of 2D **6** *Pbcm* HNC under various strains at the HSE06//PBE level of theory.

S10 2D isoelectronic XAN compounds (X=H, F; A = C, Si, Ge)

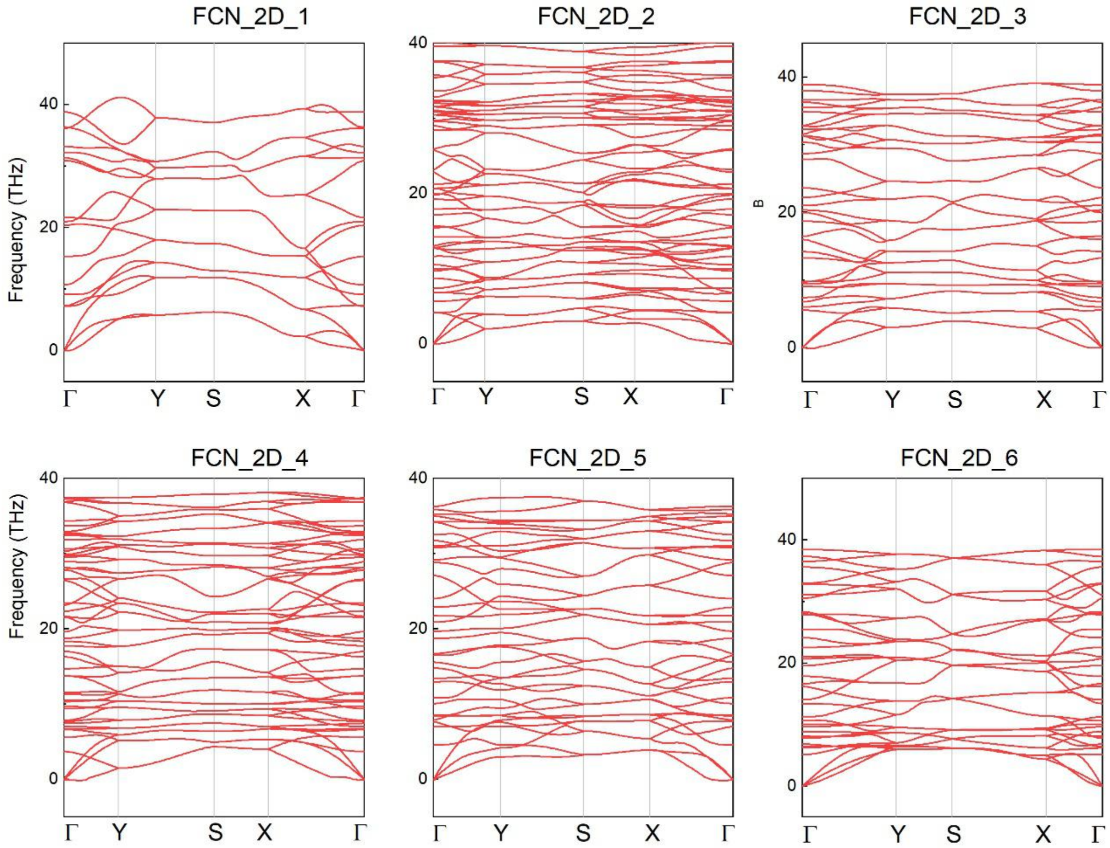

Figure S45 Phonon dispersions curves of 2D FCN compounds

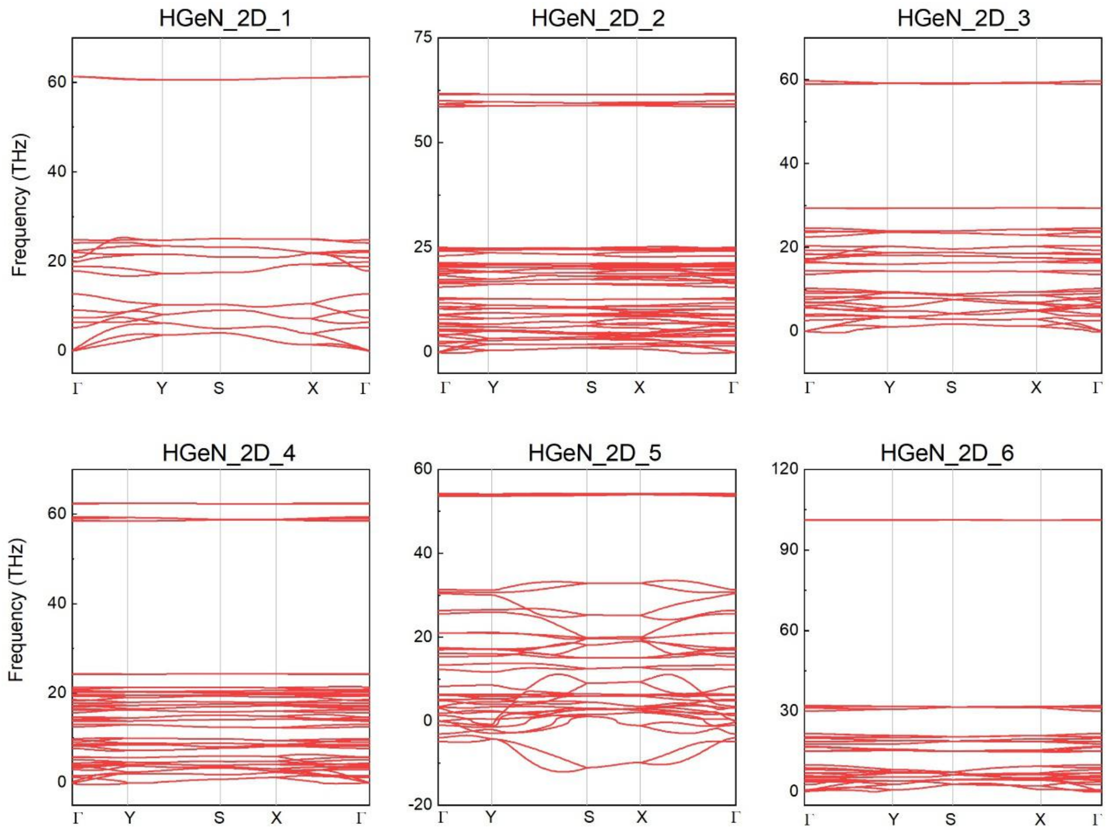

Figure S46 Phonon dispersions curves of 2D HGeN compounds. HGeN_2D_5 is not dynamically stable, due to the imaginary modes in its phonon dispersion curve.

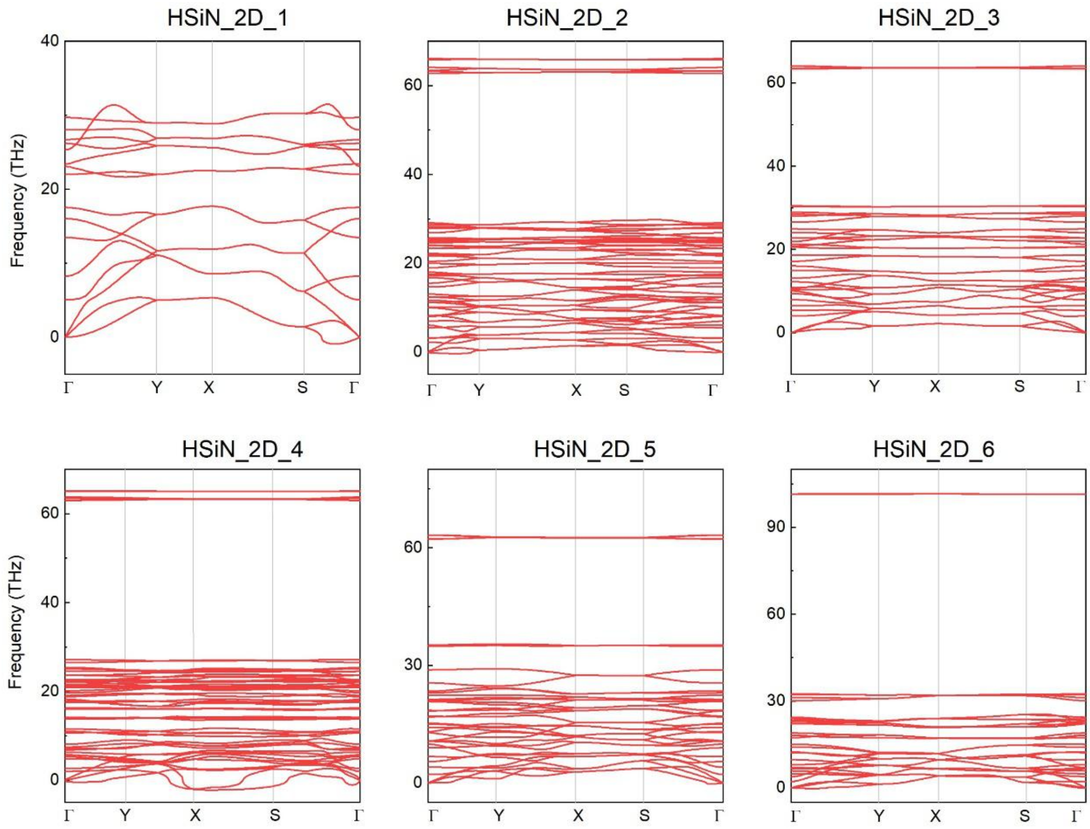

Figure S47 Phonon dispersions curves of 2D HSiN compounds. HSiN_2D_4 is not dynamically stable, due to the imaginary modes in its phonon dispersion curve.

Table S8 Calculated enthalpies, ZPEs, and crystallographic parameters of dynamically stable 2D FCN compounds at the PBE level of theory

phase	Z	Space Group	Enthalpy (eV/f.u.)	ZPE (eV/f.u..)	Lattice parameters (Å,º)	Atomic coordinates (fractional)
2D_1	2	*Pmn*2$_1$ SG 31	-20.805	0.392	a= 2.418, b=21.685, c=3.795, α=β=γ=90.0	N 2a (0.500 0.018 0.152) C 2a (0.500 0.974 0.862) F 2a (0.500 0.914 0.993)
2D_2	6	*Pma*2 SG 28	-20.407	0.394	a=7.275, b=3.823, c=37.269, α=β=γ=90.0	C 4d (0.088 0.885 0.743) C 2c (0.250 0.391 0.773) F 4d (0.091 0.755 0.708) F 2c (0.250 0.264 0.808) N 4d (0.082 0.605 0.769) N 2c (0.250 0.097 0.748)
2D_3	4	*P*2$_1$2$_1$2 SG 18	-20.411	0.394	a=3.783, b=4.811, c=38.048, α=β=γ=90.0	N 4c (0.395 0.120 0.991) C 4c (0.889 0.858 0.017) F 4c (0.767 0.819 0.050)
2D_4	6	*Cm*	-20.063	0.396	a=7.309, b=4.154,	C 1a (0.828 0.303 0.049)

		SG 8			c=39.166, α=β=γ=90.0	C 1a (0.328 0.803 0.049) C 1a (0.172 0.303 0.049) C 1a (0.672 0.803 0.049) C 1a (0.500 0.618 0.036) C 1a (0.000 0.118 0.036) F 1a (0.836 0.303 0.085) F 1a (0.336 0.803 0.085) F 1a (0.164 0.303 0.085) F 1a (0.664 0.803 0.085) F 1a (0.500 0.624 0.000) F 1a (0.000 0.124 0.000) N 1a (0.667 0.131 0.037) N 1a (0.167 0.631 0.037) N 1a (0.333 0.131 0.037) N 1a (0.833 0.631 0.037) N 1a (0.500 0.299 0.050) N 1a (0.000 0.799 0.050)
2D_5	4	$P222_1$ SG 17	-19.644	0.393	a= 4.816, b=39.999, c=3.887, α=β=γ=90.0	N 4e (0.116 0.985 1.137) C 4e (0.636 0.985 1.142) F 4e (0.653 0.955 0.983)
2D_6	4	*Pbcm* SG 57	-18.269	0.395	a= 22.999, b=2.845, c=4.760, α=β=γ=90.0	N 4d (0.054 0.313 0.250) F 4d (0.108 0.069 0.250) C 4c (0.020 0.250 0.500)

Table S9 Calculated enthalpies, ZPEs, and crystallographic parameters of dynamically stable 2D HGeN compounds at the PBE level of theory

phase	Z	Space Group	Enthalpy (eV/f.u.)	ZPE (eV/f.u.)	Lattice parameters (Å,º)	Atomic coordinates (fractional)
2D_1	2	$Pmn2_1$ SG 31	-16.086	0.335	a=3.080, b=21.533, c=4.802, α=β=γ=90.0	N 2a (1.000 0.021 0.837) Ge 2a (1.000 0.964 0.132) H 2a (1.000 0.897 0.021)
2D_2	6	*Pma*2 SG 28	-15.052	0.337	a=9.366, b=4.770, c=33.753, α=β=γ=90.0	Ge 4d (0.093 0.837 0.734) Ge 2c (0.250 0.355 0.785) H 4d (0.126 0.695 0.693) H 2c (0.250 0.248 0.829) N 4d (0.069 0.575 0.776) N 2c (0.250 0.055 0.748)

2D_3	4	*P*2$_1$2$_1$2 SG 18	-15.100	0.339	a=4.793, b=6.162, c=23.445, α=β=γ=90.0	Ge 4c (0.356 0.667 0.042) H 4c (0.235 0.751 0.100) N 4c (0.566 0.896 0.011)
2D_4	6	*Cm* SG 8	-14.561	0.336	a=9.150, b=5.472, c=33.614 α=β=γ=90.0	Ge 1a (0.806 0.326 0.053) Ge 1a (0.306 0.826 0.053) Ge 1a (0.194 0.326 0.053) Ge 1a (0.694 0.826 0.053) Ge 1a (0.500 0.577 0.027) Ge 1a (0.000 0.077 0.027) H 1a (0.798 0.333 0.100) H 1a (0.298 0.833 0.100) H 1a (0.202 0.333 0.100) H 1a (0.702 0.833 0.100) H 1a (0.500 0.556 0.981) H 1a (0.000 0.056 0.981) N 1a (0.636 0.158 0.032) N 1a (0.136 0.658 0.032) N 1a (0.364 0.158 0.032) N 1a (0.864 0.658 0.032) N 1a (0.500 0.247 0.051) N 1a (0.000 0.747 0.051)
2D_6	4	*Pbcm* SG 57	-14.758	0.337	a= 22.051, b=4.195, c=6.137, α=β=γ=90.0	N 4d (0.081 0.781 0.250) H 4d (0.112 0.598 0.250) Ge 4c (0.968 0.250 0.500)

Table S10 Calculated enthalpies, ZPEs, and crystallographic parameters of dynamically stable 2D HSiN compounds at the PBE level of theory

phase	Z	Space Group	Enthalpy (eV/f.u.)	ZPE (eV/f.u.)	Lattice parameters (Å,°)	Atomic coordinates (fractional)
2D_1	2	*Pmn*2$_1$ SG 31	-19.007	0.405	a=2.906, b=24.443, c=4.798, α=β=γ=90.0	N 2a (0.500 0.009 0.803) Si 2a (0.500 0.974 0.123) H 2a (0.500 0.914 0.067)
2D_2	6	*Pma*2 SG 28	-17.542	0.406	a=8.845, b=4.711, c=36.186, α=β=γ=90.0	Si 4d (0.095 0.844 0.739) Si 2c (0.250 0.351 0.780) H 4d (0.116 0.737 0.700) H 2c (0.250 0.267 0.819) N 4d (0.080 0.560 0.770)

						N 2c (0.250 0.047 0.751)
2D_3	4	$P2_12_12$ SG 18	-17.338	0.404	a=4.740, b=5.851, c=29.467, α=β=γ=90.0	Si 4c (0.859 0.831 0.029) H 4c (0.773 0.757 0.076) N 4c (0.439 0.115 0.995)
2D_5	4	$P222_1$ SG 17	-16.496	0.405	a= 4.517, b=45.004, c=3.859, α=β=γ=90.0	N 4e (0.898 0.987 0.403) Si 4e (0.647 0.957 0.493) H 4e (0.809 0.929 0.544)
2D_6	4	*Pbcm* SG 57	-16.170	0.402	a= 22.302, b=3.934, c=5.847, α=β=γ=90.0	N 4d (0.075 0.769 1.250 H 4d (0.108 0.585 1.250) Si 4c (0.969 0.250 0.500)

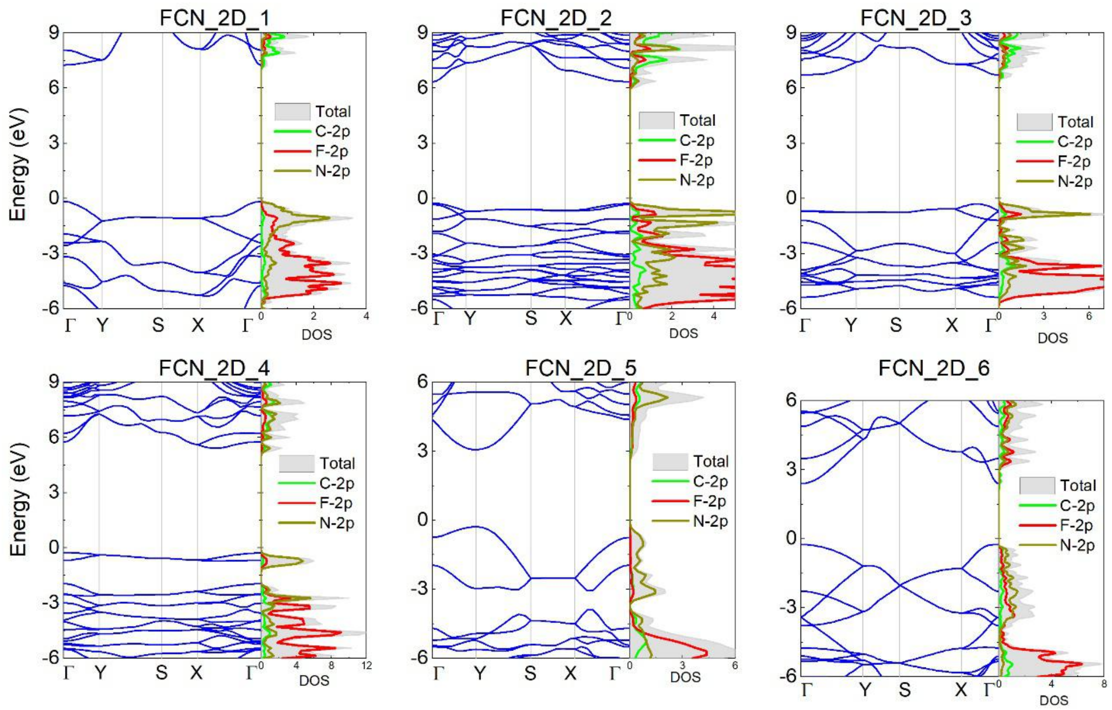

Figure S48 Calculated band structures and DOS of 2D FCN_2D_**1**, **2**, **3**, **4**, **5**, and **6** at the HSE06//PBE level of theory. The Fermi energy is set to zero. The energy band gaps are 7.4, 6.6, 7.0, 5.7, 3.3, and 2.6 eV, respectively.

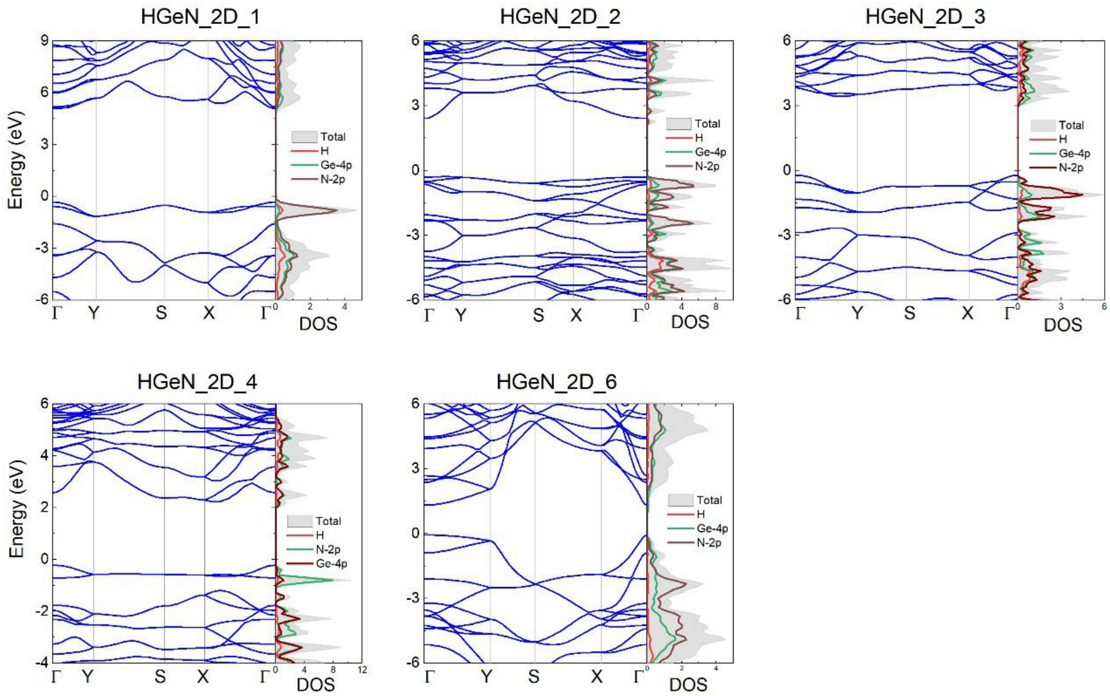

Figure S49 Calculated band structures and DOS of 2D HGeN_2D_**1**, **2**, **3**, **4**, and **6** at the HSE06//PBE level of theory. The band gaps are 5.4, 2.7, 3.6, 2.4, and 1.4, respectively.

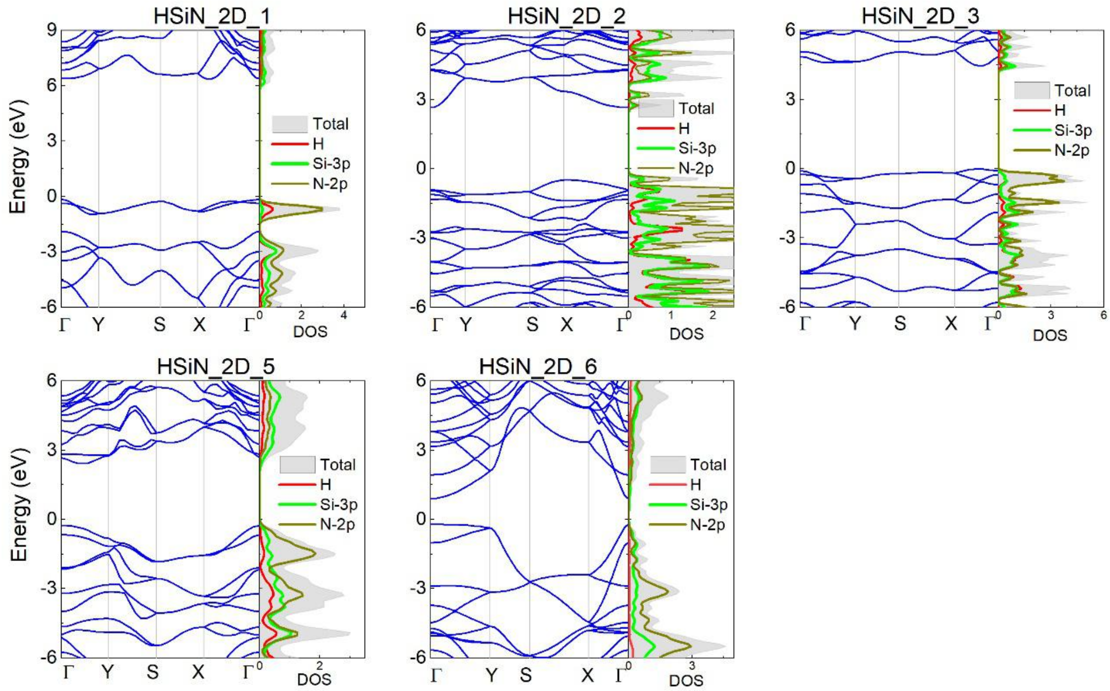

Figure S50 Calculated band structures and DOS of 2D HSiN_2D_**1**, **2**, **3**, **5** and **6** at the HSE06//PBE level of theory. The band gaps are 6.6, 2.9, 4.5, 3.5, and 1.1 eV, respectively.

S11 AIMD simulations on molecular polymerization reaction

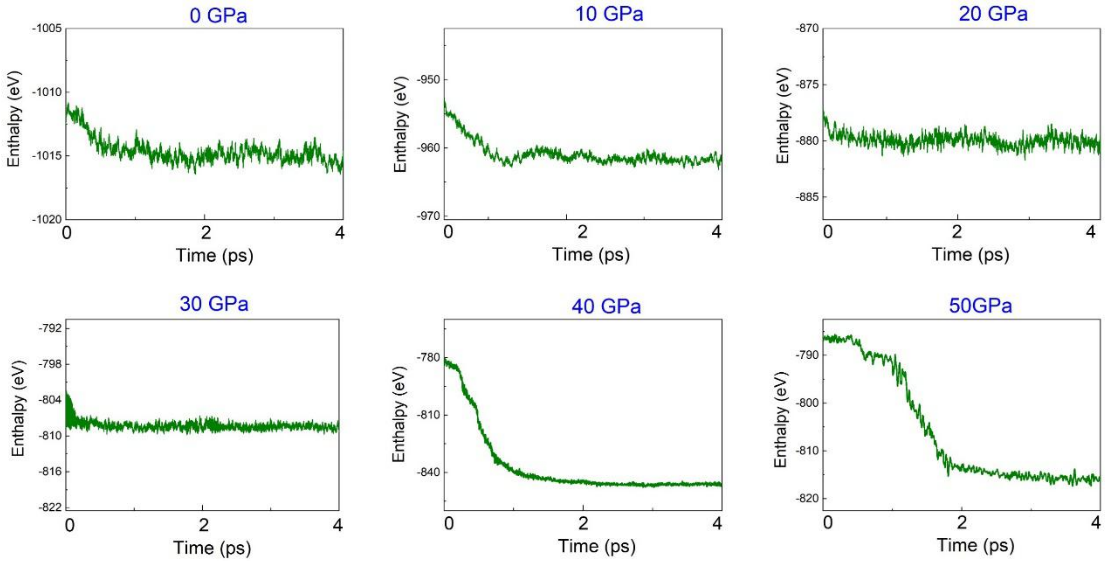

Figure S51 Energy fluctuations of bulk 3×3×3 *I*4*mm* HCN supercell during the AIMD simulations at 0, 10, 20, 30, 40, and 50 GPa.

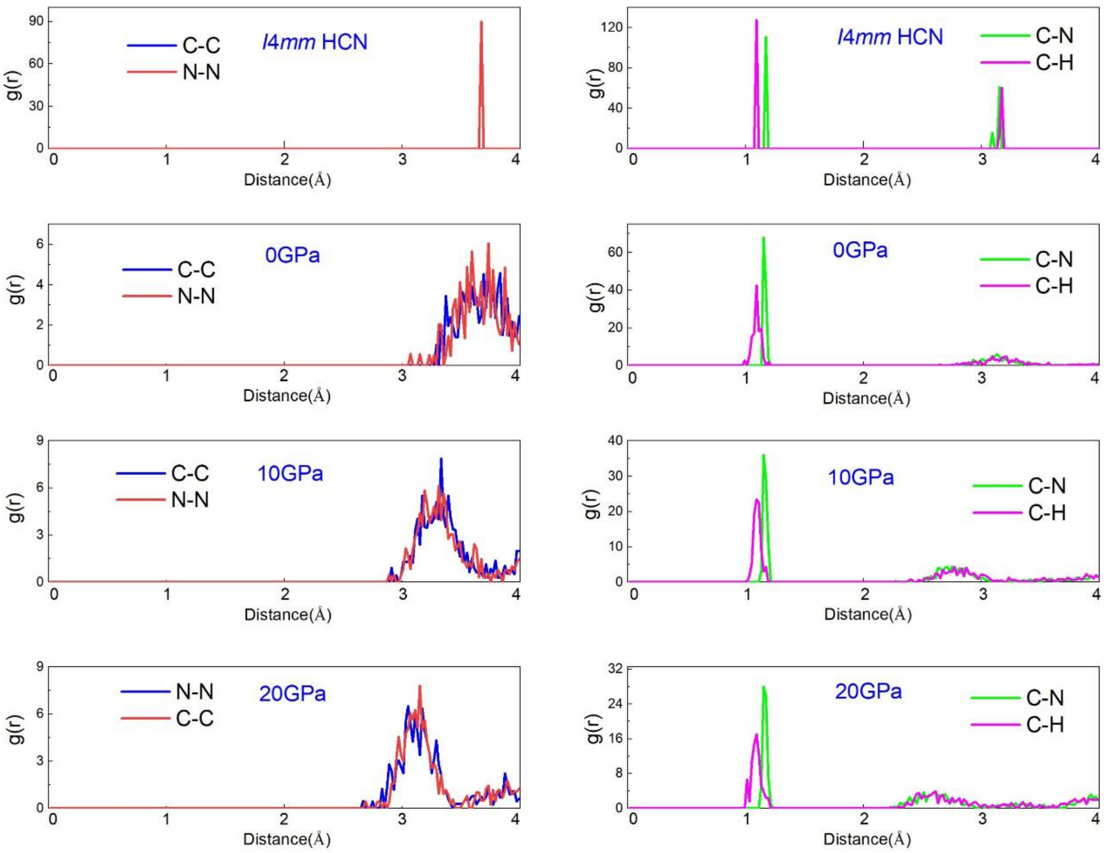

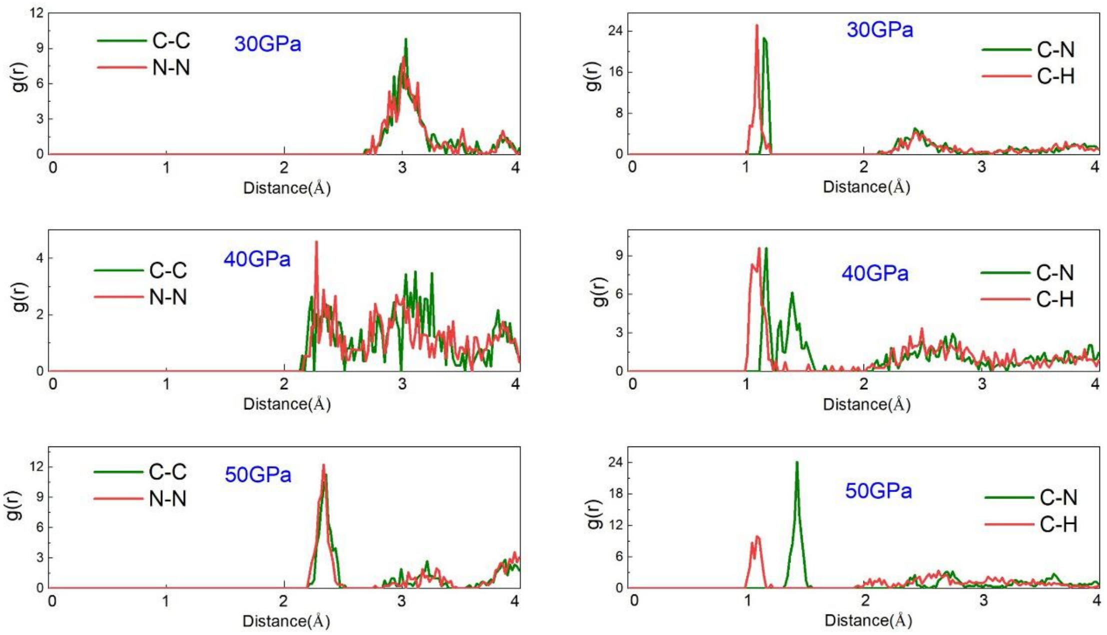

Figure S52 Radial distribution functions (RDFs) $g(r)$ of the C-C, N-N, C-N, and C-H distances observed during AIMD simulations at 0, 10, 20, 30, 40, and 50 GPa in bulk 3×3×3 *I*4*mm* HCN supercell.

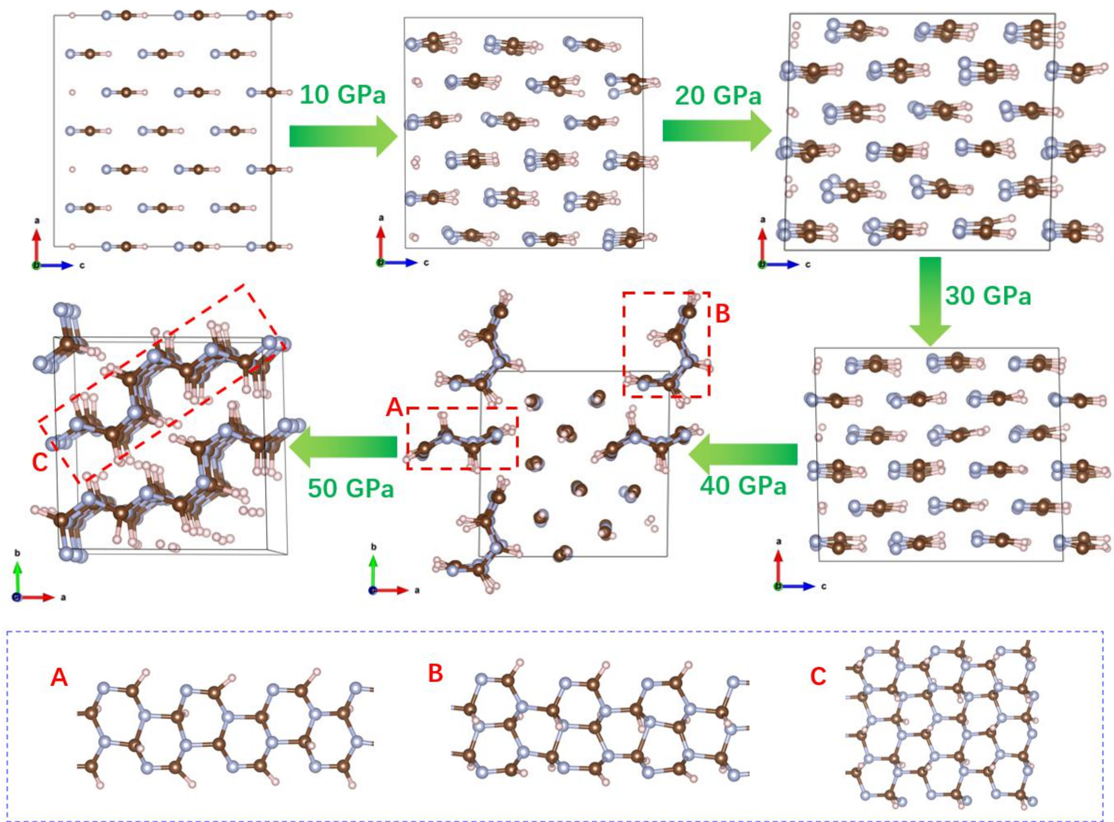

Figure S53 Polymerization reaction from *I*4*mm* HCN crystal to 2D HCN covalent nets during AIMD simulations at 0-50 GPa and 400K

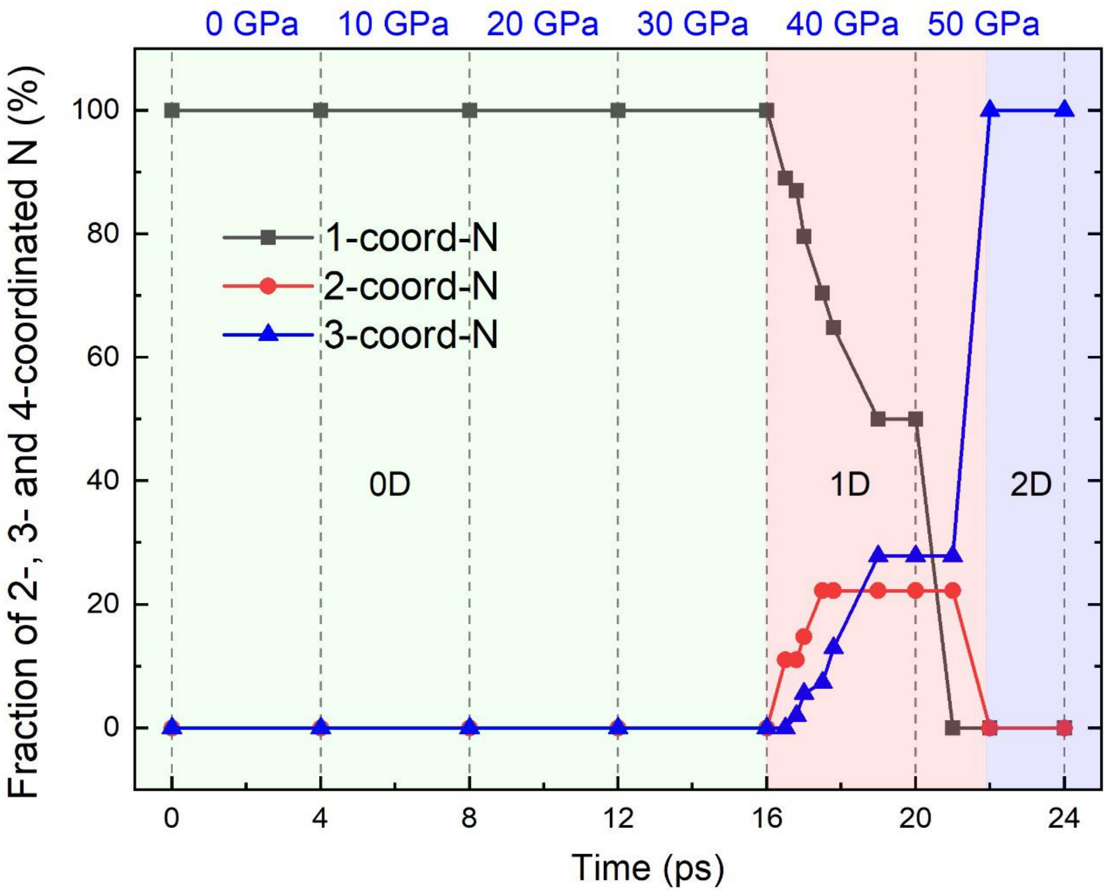

Figure S54 Concentration of nitrogen coordination states at different pressures from AIMD simulations at 400 K

S12 References

1. A. R. Oganov and C. W. Glass, *J. Chem. Phys*., 2006, **124**, 244704.
2. A. R. Oganov, A. O. Lyakhov and M. Valle, *Accounts Chem. Res*., 2011, **44**, 227-237.
3. A. O. Lyakhov, A. R. Oganov, H. T. Stokes and Q. Zhu, *Comput. Phys. Commun*., 2013, **184**, 1172-1182.
4. X. F. Zhou, X. Dong, A. R. Oganov, Q. Zhu, Y. Tian and H. T. Wang, *Phys. Rev. Lett*., 2014, **112**, 085502.
5. B. Dong, Z. Wang, N. T. Hung, A. R. Oganov, T. Yang, R. Saito and Z. Zhang, *Phys. Rev. Mater.*, 2019, **3**, 013405.
6. G. Kresse and J. Furthmüller, *Comput. Mater. Sci*., 1996, **6**, 15-50.
7. G. Kresse and J. Furthmüller, *Phys. Rev. B*, 1996, **54**, 11169.
8. J. O. Sofo, A. S. Chaudhari and G. D. Barber, *Phys. Rev. B*, 2007, **75**, 153401.
9. C. He, C. X. Zhang, L. Z. Sun, N. Jiao, K. W. Zhang and J. Zhong, *Phys. Status Solidi Rapid Res. Lett*., 2012, **6**, 427-429.
10. S. Marutheeswaran, P. D. Pancharatna and M. M. Balakrishnarajan, *Phys. Chem. Chem. Phys*., 2014, **16**, 19861-19865.
11. P. E. Blöchl, *Phys. Rev. B*, 1994, **50**, 17953.
12. J. P. Perdew, K. Burke and M. Ernzerhof, *Phys. Rev. Lett*., 1998, **80**, 891.
13. J. Hafner, *J. Comput. Chem.,* 2008, **29**, 2044-2078.
14. J. Heyd, G. E. Scuseria and M. Ernzerhof, *J. Chem. Phys*., 2003, **118**, 8207-8215.
15. T. A. Manz and N. G.Limas, *RSC Adv*., 2016, **6**, 47771-47801.
16. K. Momma and F. Izumi, *J. Appl. Crystallogr*., 2011, **44**, 1272-1276.
17. A. Togo, F. Oba and I. Tanaka,. *Phys. Rev. B*, 2008, **78**, 134106.
18. M. Born, K.Huang, and M. Lax, *Am. J. Phys*., 1955, **23**, 474-474.
19. R. Cowley, *Phys. Rev. B*, 1976, **13**, 4877.
20. F. Mouhat and F. X.Coudert, *Phys. Rev. B*, 2014, **90**, 224104.
21. Y. L. Page and P. Saxe, *Phys. Rev. B*, 2002, **65**, 104104.
22. C. Jasiukiewicz, T. Paszkiewicz and S. Wolski, *Phys. Status Solidi B*, 2008, **245**, 557-561.
23. M. K. Mohanta, A. Rawat, Dimple, N. Jena, R. Ahammed and A. De Sarkar, *Nanoscale*, 2019, **11**, 21880-21890.
24. L. Wang, A. Kutana, X. Zou and B. I. Yakobson, *Nanoscale*, 2015, **7**, 9746-9751.
25. M. K. Mohanta, A. Kishore and A. De Sarkar, *Nanotechnology*, 2020, **31**, 495208.

26. S. Grimme, *J. Comput. Chem*., 2006, **27**, 1787-1799.
27. M. Parrinello and A. Rahman, *Phys. Rev. Lett*., 1980, **45**, 1196.
28. M. Parrinello and A. Rahman, *J. Appl. Phys*., 1981, **52**, 7182-7190.
29. J. Yan, O. Tóth, W. Xu, X. D. Liu, E. Gregoryanz, P. Dalladay-Simpson, Z. Qi, S. Xie, F. Gorelli and R. Martonak, *J. Phys. Chem. Lett.,* 2021, **12**, 7229-7235.
30. H. Zhang, O. Tóth, X. D. Liu, R. Bini, E. Gregoryanz, P. Dalladay-Simpson, S. De Panfilis, M. Santoro, F. A. Gorelli and R. Martoňák, *Proc. Natl. Acad. Sci. U.S.A*., 2020, **117**, 8736-8742.
31. D. M. Koch, C. Toubin, S. Xu, G. H. Peslherbe and J. T. Hynes, *J. Phys. Chem. C,* 2007, **111**, 15026-15033.
32. P. Coppens, *Science,* 1967, **158**, 1577-1579.
33. H. Neunhoeffer, M.Clausen, H. D. Vötter, H. Ohl, C. Krüger and K. Angermund, *Liebigs Ann. Chem.,* 1985, **1985**, 1732-1751.
34. W. Dulmage and W. Lipscomb, *Acta Crystallogr.,* 1951, **4**, 330-334.
35. M. Khazaei, Y. Liang, M. S. Bahramy, F. Pichierri, K. Esfarjani and Y. Kawazoe, *J. Phys. Condens. Matter,* 2011, **23**, 405403.
36. W. Yi, T. Hu, T. Su, R. Islam, M. Miao and J. Liu, *J. Mater. Chem. C,* 2017, **5**, 8498-8503.
37. S. Yoo, B. Lee and K. Kang, *Nanotechnology,* 2021, **32**, 295702.
38. Q. Peng, X. Wen, and S. De, *RSC Adv.,* 2013, **3**, 13772-13781.
39. J. Li, T. Zhao, C. He and K. Zhang, *J. Phys. D: Appl. Phys.,* 2018, **51**, 12LT01.
40. G. Zheng, Y. Jia, S. Gao and S. H. Ke, *Phys. Rev. B*, 2016, **94**, 155448.
41. C. Ataca, H. Sahin, E. Akturk and S. Ciraci, *J. Phys. Chem. C,* 2011, **115**, 3934-3941.
42. K. A. N. Duerloo, M. T. Ong and E. J. Reed, *J. Phys. Chem. Lett.,* 2012, **3**, 2871-2876.